

# Modeling carbon and silicon cycling in the equatorial Pacific

Masahiko Fujii\*, Fei Chai

*School of Marine Sciences, University of Maine, 5706 Aubert Hall, Orono, ME 04469-5706, USA*

Accepted 10 December 2006  
Available online 12 March 2007

## Abstract

The equatorial Pacific is a region of significant particulate inorganic carbon (PIC) and biogenic silica sedimentation, the majority of which is carried out by coccolithophorids and diatoms. We developed an ecosystem model that explicitly includes three phytoplankton functional groups (picoplankton, coccolithophorids, and diatoms), two zooplankton functional groups (microzooplankton and mesozooplankton), nutrients (nitrate  $\text{NO}_3$ , ammonium  $\text{NH}_4$ , and silicate  $\text{Si}(\text{OH})_4$ ), detritus (particulate organic matter, biogenic silica, and PIC), total alkalinity, total  $\text{CO}_2$ , and partial pressure of  $\text{CO}_2$  at the surface water ( $\text{pCO}_{2\text{sea}}$ ). The model is capable of reproducing many biogeochemical features for the region, such as high-nutrient low-chlorophyll condition, significant exposure of phytoplankton under grazing controls by zooplankton, and large  $\text{CO}_2$  release to the atmosphere. The export ratio of PIC to particulate organic carbon (rain ratio) to the deep water was 0.16, higher than the global-mean values, implying predominant PIC sedimentation in the equatorial Pacific upwelling region. Comparison between calcification and no-calcification model results indicates that when coccolithophorids are present, the community interactions actually induce more diatom biomass, export fluxes of detritus, and  $\text{CO}_2$  release to the atmosphere. The model results show remarkable calcification in the subsurface layers, which suggests more field data on calcification processes are needed. Increase of source (120 m depth)  $\text{Si}(\text{OH})_4$  concentration associated with the tropical instability waves lead to a linear increase in biogenic silica export. Higher  $\text{Si}(\text{OH})_4$  concentration stimulates diatom growth, which causes a decrease in picoplankton because feeding pressure by mesozooplankton switched from picoplankton's grazer, microzooplankton, to the abundant diatoms. Surface coccolithophorid biomass has its maximum at intermediate source  $\text{Si}(\text{OH})_4$  concentrations as a result of higher grazing pressure on coccolithophorids and higher  $\text{NO}_3$  regulation on coccolithophorid growth, with lower and higher source  $\text{Si}(\text{OH})_4$  concentrations, respectively. Surface total alkalinity has its minimum and  $\text{TCO}_2$  has its maximum at intermediate source  $\text{Si}(\text{OH})_4$  concentrations. The two effects on  $\text{pCO}_{2\text{sea}}$  result in maximum  $\text{CO}_2$  release to the atmosphere and PIC export to the deep water, with nearby standard source  $\text{Si}(\text{OH})_4$  concentration of  $7.5 \text{ (mmol Si m}^{-3}\text{)}$ . The enhanced changes in biogenic silica export flux than in surface diatom biomass, confirmed by the model sensitivity study, suggest sedimented detritus under the equatorial Pacific upwelling region acts as an amplifier of changes in surface properties. The model results suggest that physical forcing, such as tropical instability waves, Kelvin waves, and La Niña, which is capable of changing  $\text{Si}(\text{OH})_4$  and iron concentrations in the euphotic zone, significantly affect both carbon and silicon fluxes in the region.

© 2007 Elsevier Ltd. All rights reserved.

*Keywords:* Carbon cycle; Silicon cycle; Coccolithophorids; Grazing; Modeling; Equatorial Pacific

\*Corresponding author. Now at Sustainability Governance Project, Creative Research Initiative "Sousei", Hokkaido University, Sapporo, Hokkaido 060-0809, Japan. Tel.: +81 11 706 4536; fax: +81 11 706 4534.

E-mail address: [mfujii@sgp.hokudai.ac.jp](mailto:mfujii@sgp.hokudai.ac.jp) (M. Fujii).

## 1. Introduction

### 1.1. Calcification in the equatorial Pacific

Calcifying plankton have a great role in oceanic carbon cycling and global climate change because of particulate inorganic carbon (PIC) shell production resulting in reduced alkalinity and CO<sub>2</sub> release to the atmosphere, the ballasting effect of carbonate minerals, and the packaging effect of promoting the transfer of organic carbon to the deep sea (e.g., Armstrong et al., 2002; Francois et al., 2002).

Previous studies have indicated that the majority (80%) of global marine biogenic carbonate precipitation is carried out by coccolithophorids (Deuser and Ross, 1989; Fabry, 1989; Westbroek et al., 1989) through their production of PIC coccoliths. Coccolithophorids act as a significant biotic source of dimethyl sulfide (DMS) for the atmosphere and may influence regional albedo via increased cloud formation (Bates et al., 1987; Charlson et al., 1987; Brown and Yoder, 1994). The coccolithophorid bloom affects physical environments through changing albedo due to their unique light scattering properties, and biogeochemical processes from lower to higher trophic levels. The progressive increase in atmospheric CO<sub>2</sub> concentrations predicted for the next few decades will decrease the production of PIC in the surface ocean (Riebesell et al., 2000; Orr et al., 2005), and thus this response could potentially act as a negative feedback on atmospheric CO<sub>2</sub> levels (Iglesias-Rodríguez et al., 2002).

Although satellite-based estimates of coccolithophore blooms appear in high-latitude oceans, and the relative paucity of such blooms in the tropics (Holligan et al., 1983; Brown and Yoder, 1994; Brown, 1999; Iglesias-Rodríguez et al., 2002), the equatorial Pacific is known as a region of significant PIC sedimentation (van Andel, 1975), which represents 12–19% of global PIC production, and is on the same order of magnitude as new production in this region (Chavez and Barber, 1987; Balch and Kilpatrick, 1996). The equatorial Pacific is a largest natural CO<sub>2</sub> source to the atmosphere, and therefore change in calcification in the region can significantly impact on the global carbon cycling.

Calcification in the equatorial Pacific is poorly understood from ecological and biogeochemical perspectives because direct field estimates of calcification are few (Balch and Kilpatrick, 1996). Ecosystem modeling can help us to fill the gaps in

observations and interpret observed results. Several ecosystem models have incorporated calcifying plankton as well as carbonate system (Fujii et al., 2002; Moore et al., 2002; Pätsch et al., 2002; Yamanaka et al., 2004). However, they all assumed a constant composition ratio of coccolithophorids to total phytoplankton or a constant ratio of calcification to net community production. Only very few previous studies have incorporated calcifying plankton in their models as an independent state variable (Pasquer et al., 2005; Buitenhuis et al., 2006).

### 1.2. Silicification in the equatorial Pacific

The equatorial Pacific upwelling region is known as one of the major high-nutrient, low-chlorophyll (HNLC) regions. This oceanic region is also characterized by permanently lower Si(OH)<sub>4</sub> than NO<sub>3</sub> concentration. For example, typical source (120 m depth) concentration is 7.5 (mmol Si m<sup>-3</sup>) for Si(OH)<sub>4</sub> and 12.5 (mmol Si m<sup>-3</sup>) for NO<sub>3</sub>, which leads to lower surface Si(OH)<sub>4</sub> than NO<sub>3</sub> concentration and potential Si(OH)<sub>4</sub> limitation on the diatom growth (Ku et al., 1995; Dugdale et al., 1995; Dugdale and Wilkerson, 1998). However, field data in this region have shown that the source Si(OH)<sub>4</sub> concentration ranges substantially from 3 to 13 (mmol Si m<sup>-3</sup>) (e.g., Dugdale et al., 2002). This means that the Si(OH)<sub>4</sub> limitation on the diatom growth and, therefore, phytoplankton community composition could change widely in response to the source Si(OH)<sub>4</sub> concentration. Recent iron enrichment experiments in the equatorial Pacific have shown that iron as well as Si(OH)<sub>4</sub> concentration are crucial factors determining diatom growth and its biomass accumulation (Martin et al., 1994; Coale et al., 1996; Price et al., 1994; Sanderson et al., 1995).

Both Si(OH)<sub>4</sub> and iron in the surface water are primarily supplied by upwelling from the deep water (Chavez et al., 1991; Dugdale et al., 2002), although less is known of the distribution of iron, its form, and cycling. The nutrient concentrations change with physical forcing that varies on different time scales from days to years. Several previous studies have investigated biogeochemical responses in the equatorial Pacific to the non steady-state event associated with the passage of the tropical instability waves (TIWs), La Niña and Kelvin waves (Barber et al., 1996; Foley et al., 1996; Dunne et al., 1999; Dugdale et al., 2002). The passage of the

TIWs lifts isopycnals, presumably elevating  $\text{Si(OH)}_4$  and iron concentrations, as well as diatom production in the euphotic zone for a short period (Flament et al., 1996; Archer et al., 1997). The passage of Kelvin waves, by contrast, depresses the thermocline (Kessler and McPhaden, 1995), decreasing inputs of iron to the euphotic zone.

Although the concept of non-steady-state is important in understanding equatorial biogeochemical cycles (Dunne et al., 1999), the total impact of the TIWs and Kelvin waves and their frequency still remains uncertain mainly due to a paucity of field data. In parallel, several modeling studies have examined the biological responses to enhanced nutrients by the TIWs. Using a 10-compartment ecosystem model that fully incorporates silicon cycling, and representing iron enrichment by changing two photosynthetic parameters of the diatoms, Chai et al. (2002) reproduced several ecological behaviors similar to those observed during the second mesoscale iron enrichment experiment (IronExII; at 3.5°S, 104°W). These behaviors included a rapid increase in diatom growth and biomass, termination of the iron-induced diatom bloom due to exhaustion of available iron and  $\text{Si(OH)}_4$ , and increased mesozooplankton population as a grazer on diatoms. Using the same ecosystem model, Dugdale et al. (2002) suggested that the stability of the equatorial system with its narrow range of biological and chemical variables is conferred by the action of diatoms providing food for mesozooplankton, whose grazing also depletes picoplankton. They also suggested that diatoms increase while picoplankton population and  $\text{NO}_3$  consumption decrease with source  $\text{Si(OH)}_4$  increases. As a result, a maximum surface total carbon dioxide ( $\text{TCO}_2$ ) and increased  $\text{CO}_2$  flux to the atmosphere appear at intermediate source  $\text{Si(OH)}_4$  concentrations.

### 1.3. Objective of this study

To elucidate factors that affect calcification and PIC sedimentation in the equatorial Pacific, we propose to address the roles of coccolithophorids and other phytoplankton and zooplankton groups that affect coccolithophorids. We develop and use an ecosystem model incorporating coccolithophorids, PIC, and total alkalinity. The model performance is tested by applying the model to the equatorial Pacific upwelling region. Model sensitivity analysis to biogeochemical parameters (Experi-

ment 1) is conducted to understand dominant biological processes in the newly-developed ecosystem model.

To examine responses of the biogeochemistry in the equatorial Pacific to changes in  $\text{Si(OH)}_4$  and iron concentrations in the euphotic zone induced by the TIWs, we conduct a model sensitivity study (Experiment 2). In Experiment 2, we investigate model sensitivity to the source (120 m depth)  $\text{Si(OH)}_4$  concentrations under the steady-state conditions. We compare all the model results to those with no-calcification model simulation, as well as the JGOFS EqPac field data.

## 2. Experimental design

### 2.1. Model description

We added three prognostic variables, namely calcifying phytoplankton (coccolithophorids, or P3), total alkalinity (TAlk), and particulate inorganic carbon (PIC) (Fig. 1), as well as the other phytoplankton functional groups (picoplankton (P1) and diatoms (P2)), zooplankton (microzooplankton (Z1) and mesozooplankton (Z2)), nutrients ( $\text{NO}_3$ ,  $\text{NH}_4$  and  $\text{Si(OH)}_4$ ), detritus (particulate organic nitrogen and carbon (PON and POC) and biogenic silica ( $\text{bSiO}_2$ )), total  $\text{CO}_2$  ( $\text{TCO}_2$ ), and partial pressure of  $\text{CO}_2$  in the surface water ( $\text{pCO}_{2\text{sea}}$ ), which were embedded in a 1-D marine ecosystem model (Chai et al., 2002). The phytoplankton and zooplankton were separated by their functional groups, not only by their size but also according to their growth and vulnerability to grazing. All the phytoplankton take up  $\text{NO}_3$ ,  $\text{NH}_4$ , and  $\text{TCO}_2$  by the photosynthesis. The diatoms also utilize  $\text{Si(OH)}_4$  for their silicification process, and the coccolithophorids take up TAlk as well as  $\text{TCO}_2$  for its calcification process. The microzooplankton graze on picoplankton. The mesozooplankton feed on diatoms, coccolithophorids, microzooplankton and PON. The explicit representation of TAlk and  $\text{TCO}_2$  in the model allows us to calculate  $\text{pCO}_{2\text{sea}}$  and the air-sea  $\text{CO}_2$  flux. The phytoplankton carbon-chlorophyll-a ratio by weight was fixed to 50. The governing equations and formulations of biogeochemical processes were denoted in Appendix A.

The model was applied to 5°S–5°N, 90–180°W (the “Wyrтки Box”, Wyrтки, 1981; Chai et al., 2002). The physical forcing is the same, and most of the biogeochemical parameter values are the same as

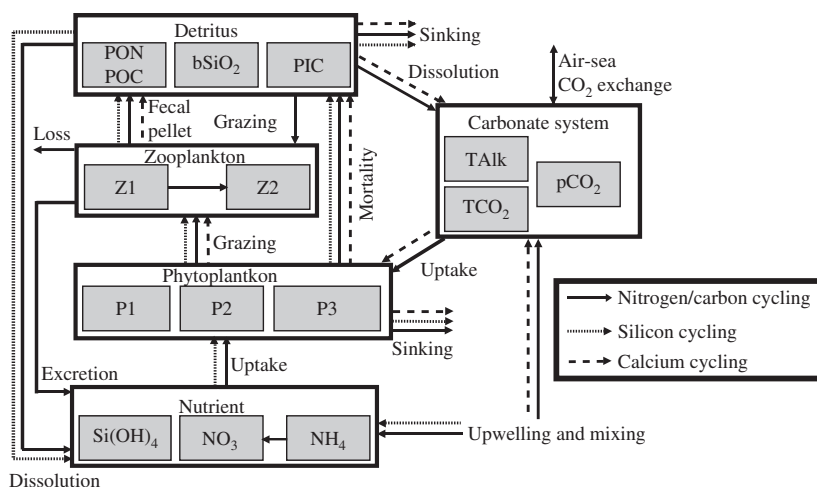


Fig. 1. The inter-compartmental flow chart of the ecosystem and linkage to physical processes. The flows of nitrogen or carbon are indicated by solid lines, the flows of silicon are indicated by dashed lines, and the flows of calcium are indicated by line-dashed lines. P1: picoplankton, P2: diatoms, P3: coccolithophorids, Z1: microzooplankton, and Z2: mesozooplankton.

Chai et al. (2002) (Table 1). The parameter values were obtained to reproduce the temporally-averaged observed constituents such as nutrient concentrations and new production in the euphotic layer (Chai et al., 1996), which varied between El Niño and non-El Niño periods (McCarthy et al., 1996). Steady-state results obtained by running the model up to 1000 days with the constant vertical velocity and diffusivity were used.

## 2.2. Data description

Data sets were used to tune the biological parameters and to compare with model outputs. Data sets used in this study are as follows: the US JGOFS EqPac observations in February–March (Survey I; TT007), March–April (Time series I; TT008), August–September (Survey II; TT011) and October (Time series II; TT012) of 1992 (Murray et al., 1995, 1996, 1997; Balch and Kilpatrick, 1996; Barber et al., 1996); the France JGOFS fluxes in the Pacific transect (FLUPAC) in October of 1994 (Le Borgne et al., 1995; Rodier and Le Borgne, 1997); the Oligotrophie en Pacifique (OLIPAC) in November 1994 (Rainbault et al., 1999); the US Zonal Flux transect (Zonal Flux) in April–May of 1996 (Dunne et al., 1999); the Etude du Broutage en Zone Equatoriale (EBENE) cruise in October–November of 1996 (Le Borgne et al., 1998; Leynaert et al., 2001); the World Ocean Database 2001 (WOD01; Conkright et al., 2002); the IronExII field data (Coale et al., 1996; Landry et al., 2000).

## 2.3. Comparison between calcification and non-calcification model simulations

To elucidate effects of newly-introduced coccolithophorids and its calcification processes on the entire biogeochemistry in the equatorial Pacific upwelling region, we compared model results with and without components and processes that were relevant to the calcification. In the non-calcification model simulation, we have excluded state variables of coccolithophorids and PIC. The non-calcification model structure was identical to that in Chai et al. (2002) and Dugdale et al. (2002). Small differences in the model results from the previous studies were attributed to different values in several biogeochemical parameters between the studies (Table 1; Chai et al., 2002).

## 3. Results

### 3.1. Calcification model

The modeling results reasonably reproduced the measured vertical features in the biogeochemistry in the equatorial Pacific, such as consistently higher  $\text{NO}_3$  than  $\text{Si(OH)}_4$  concentration (solid line in Fig. 2(D) and (F)). The modeled picoplankton (P1) was more abundant than diatoms (P2) and coccolithophorids (P3) (solid lines in Fig. 2(A)), which has been suggested from the observations (Bidigare and Ondrusek, 1996). The modeled vertically-averaged phytoplankton abundance was  $0.15 \text{ (mmol N m}^{-3}\text{)}$  for

Table 1  
The model parameters

Parameters	Symbol	(I)	(II)	Unit	Source
Light attenuation due to water	$k_1$	0.046	0.046	$m^{-1}$	(1)
Light attenuation by phytoplankton	$k_2$	0.03	0.03	$m^{-1} (mmol N m^{-3})^{-1}$	(1)
Initial slope of the P-I curve	$\alpha$	0.025	0.025	$day^{-1} (W m^{-2})^{-1}$	(1)
Maximum specific growth rate of picoplankton	$\mu_{1max}$	2.0	2.0	$day^{-1}$	(1)
NH <sub>4</sub> inhibition parameter	$\Psi$	5.59	5.59	$(mmol N m^{-3})^{-1}$	(1)
Half-saturation for NO <sub>3</sub> uptake by picoplankton	$K_{NO_3}$	1.0	1.0	$mmol N m^{-3}$	(1)
Half-saturation for NH <sub>4</sub> uptake by picoplankton	$K_{NH_4}$	0.1	0.1	$mmol N m^{-3}$	This study
Maximum specific growth rate of diatoms	$\mu_{2max}$	3.0	3.0	$day^{-1}$	(1)
Half-saturation for Si(OH) <sub>4</sub> uptake	$K_{Si(OH)_4}$	3.0	3.0	$mmol Si m^{-3}$	(1)
Half-saturation for NH <sub>4</sub> uptake by diatoms	$K_{P2\_NH_4}$	1.0	1.0	$mmol N m^{-3}$	(1)
Diatom sinking speed	$W_1$	1.0	1.0	$m day^{-1}$	(1)
Maximum specific growth rate of coccolithophorids	$\mu_{3max}$	1.0	N/A	$day^{-1}$	This study
Half-saturation for NO <sub>3</sub> uptake by coccolithophorids	$K_{P3\_NO_3}$	1.0	N/A	$mmol N m^{-3}$	This study
Half-saturation for NH <sub>4</sub> uptake by coccolithophorids	$K_{P3\_NH_4}$	1.0	N/A	$mmol N m^{-3}$	This study
Coccolithophorid sinking speed	$W_3$	1.0	N/A	$m day^{-1}$	This study
Microzooplankton maximum specific grazing rate	$G_{1max}$	1.25	1.25	$day^{-1}$	This study
Half-saturation for microzooplankton ingestion	$K_{1gr}$	0.5	0.5	$mmol N m^{-3}$	(1)
Microzooplankton excretion rate to NH <sub>4</sub>	$reg_1$	0.2	0.2	$day^{-1}$	(1)
Mesozooplankton maximum specific grazing rate	$G_{2max}$	0.48	0.48	$day^{-1}$	This study
Mesozooplankton assimilation efficiency	$\gamma_1$	0.75	0.75		(1)
Half-saturation for mesozooplankton ingestion for diatoms, coccolithophorids, microzooplankton and PON	$K_{2gr}$	0.25	0.25	$mmol N m^{-3}$	(1)
Diatom specific mortality rate	$\gamma_3$	0.05	0.05	$day^{-1}$	(1)
Coccolithophorid specific mortality rate	$\gamma_6$	0.05	N/A	$day^{-1}$	This study
Mesozooplankton specific mortality rate	$\gamma_2$	0.05	0.05	$day^{-1}$	(1)
Mesozooplankton excretion rate to NH <sub>4</sub>	$reg_2$	0.1	0.1	$day^{-1}$	(1)
Grazing preference for diatoms	$\rho_1$	0.35	0.7	dimensionless	This study
Grazing preference for microzooplankton	$\rho_2$	0.2	0.2	dimensionless	(1)
Grazing preference for PON	$\rho_3$	0.1	0.1	dimensionless	(1)
Grazing preference for coccolithophorids	$\rho_4$	0.35	N/A	dimensionless	This study
PON remineralization rate	$\gamma_7$	0.01	0.01	$day^{-1}$	This study
bSiO <sub>2</sub> dissolution rate	$\gamma_4$	0.01	0.01	$day^{-1}$	This study
PIC dissolution rate	$\gamma_8$	0.005	N/A	$day^{-1}$	This study
PON sinking speed	$W_2$	10.0	10.0	$m day^{-1}$	(1)
bSiO <sub>2</sub> sinking speed	$W_4$	20.0	20.0	$m day^{-1}$	This study
PIC sinking speed	$W_5$	20.0	N/A	$m day^{-1}$	This study
Diatom Si:N uptake ratio	$R_{SiN}$	1.5	1.5	$mol Si (mol N)^{-1}$	(2)
Nitrification rate	$\gamma_5$	0.025	0.025	$day^{-1}$	(2)
Ratio of PIC to organic carbon in coccolithophorids	$\epsilon$	1.0	N/A	$mol C (mol C)^{-1}$	(3)
Ratio of carbon to nitrogen in phytoplankton	$R_{CN}$	6.625	6.625	$mol C (mol N)^{-1}$	(1)

Columns (I) and (II) denotes the standard values of parameters in calcification model simulation and no-calcification model simulation, respectively. Sources noted here are: (1) Chai et al. (2002); (2) Jiang et al. (2003); (3) Fujii et al. (2002).

picoplankton, 0.06 ( $mmol N m^{-3}$ ) for diatoms, and 0.03 ( $mmol N m^{-3}$ ) for coccolithophorids (Table 2). The percentage of diatoms in the total modeled phytoplankton biomass was 24%, which was slightly higher but was consistent with the observed range of 5–20% (Bidigare and Ondrusek, 1996).

The modeled vertically-averaged biomass was 0.13 ( $mmol N m^{-3}$ ) for microzooplankton (Z1) and 0.28 ( $mmol N m^{-3}$ ) for mesozooplankton (Z2)

(Table 2), indicating that mesozooplankton was more plentiful than the other plankton, and therefore possibly high grazing or predation pressure by mesozooplankton in the equatorial Pacific upwelling region. The abundance in the modeled zooplankton rapidly decreased with depth (solid lines in Fig. 2(C)), as a result of their grazing and predation being dependent on biomass of their prey (Appendix A.2).

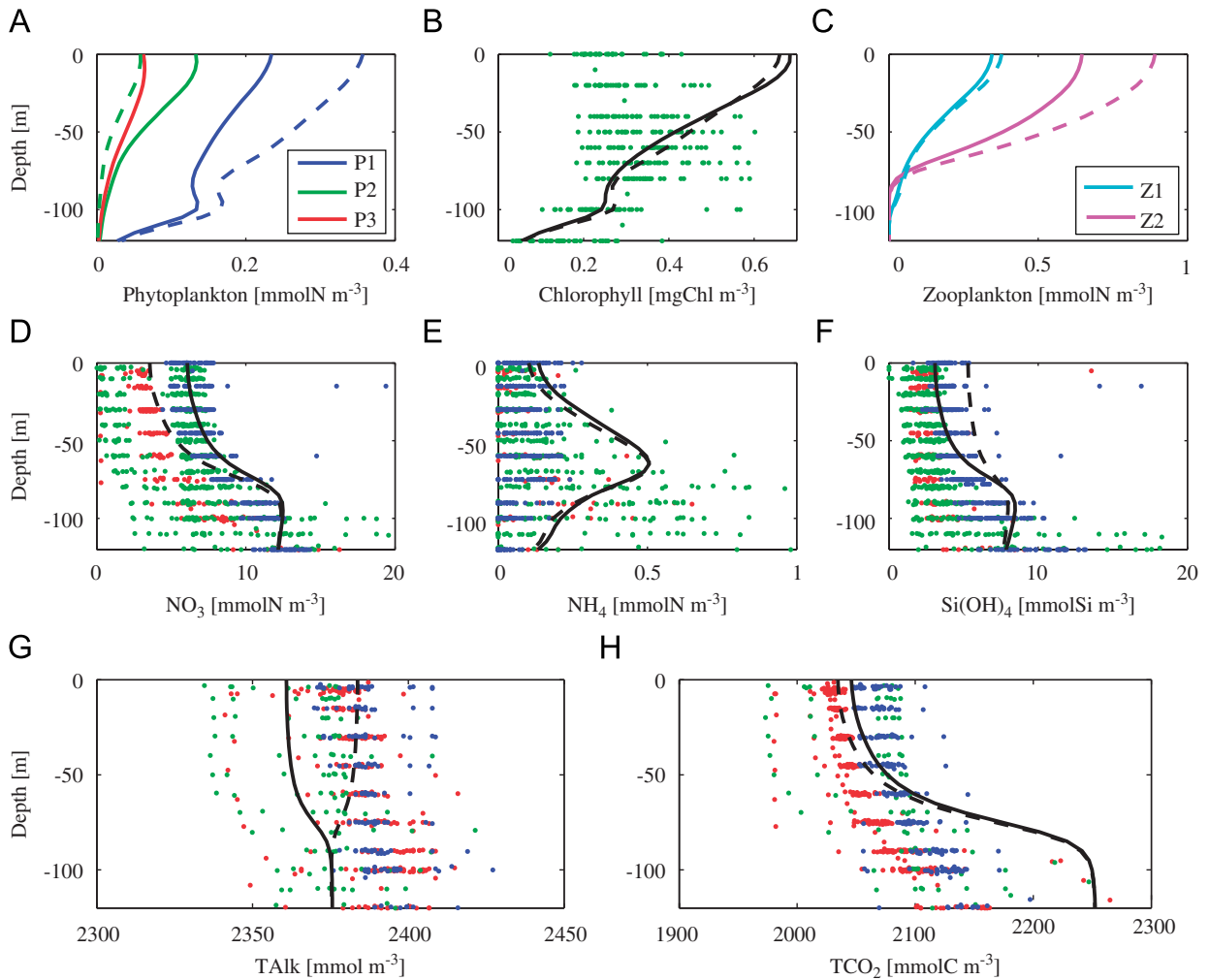


Fig. 2. Modeled vertical profiles of (A) phytoplankton biomass ( $\text{mmol N m}^{-3}$ ), (B) chlorophyll [ $\text{mgChl m}^{-3}$ ], (C) zooplankton biomass ( $\text{mmol N m}^{-3}$ ), (D)  $\text{NO}_3$  ( $\text{mmol N m}^{-3}$ ), (E)  $\text{NH}_4$  ( $\text{mmol N m}^{-3}$ ), (F)  $\text{Si(OH)}_4$  ( $\text{mmol Si m}^{-3}$ ), (G) TALK ( $\text{mmol C m}^{-3}$ ), and (H)  $\text{TCO}_2$  ( $\text{mmol C m}^{-3}$ ). Solid lines: calcification model results. Dotted lines: no-calcification model results. Dots denote the JGOFS EqPac data for TT008 (red dots), TT011 (green dots) and TT012 (blue dots).

The modeled  $\text{NO}_3$  and  $\text{Si(OH)}_4$  increased with depth (solid line in Fig. 2(D) and (F)), resulting from nutrient uptake by phytoplankton near the surface and remineralization of PON and  $\text{bSiO}_2$  below the depth. At 120 m,  $\text{Si(OH)}_4$  concentration was  $7.5$  ( $\text{mmol Si m}^{-3}$ ), whereas  $\text{NO}_3$  concentration was  $12.0$  ( $\text{mmol N m}^{-3}$ ), and these values are close to the observed climatological data, respectively (Levitus et al., 1993; Murray et al., 1995; Chai et al., 2002; Dugdale et al., 2002). The surface concentration was  $6.1$  ( $\text{mmol N m}^{-3}$ ) in  $\text{NO}_3$  and  $3.1$  ( $\text{mmol Si m}^{-3}$ ) in  $\text{Si(OH)}_4$ . The model captured the observed subsurface maximum of  $\text{NH}_4$  concentration (solid line in Fig. 2(E); Murray et al., 1995).

The subsurface  $\text{NH}_4$  maximum is due to higher uptake rate of  $\text{NH}_4$  near the surface mainly by picoplankton, which has relatively smaller half-saturation constant for  $\text{NH}_4$  uptake ( $0.1$  ( $\text{mmol N m}^{-3}$ )) than the other phytoplankton ( $1.0$  ( $\text{mmol N m}^{-3}$ )) (Table 1).

The modeled  $\text{TCO}_2$  had similar vertical profile as of nutrients, increasing with depth (solid line in Fig. 2(H)), as a result of  $\text{TCO}_2$  uptake by phytoplankton growth and calcification by coccolithophorids in the upper layer and decomposition of POC and PIC in the lower layer. The TALK was only changed by the calcification process, i.e. shell formation by coccolithophorids in the upper layer

Table 2

Vertically-averaged plankton biomass in the euphotic zone (up to 120 m) in (1) calcification model and (2) no-calcification model simulations. Composition ratio of each phytoplankton species to total phytoplankton is shown in percentage term in parentheses

Picoplankton (P1) [mmol N m <sup>-3</sup> ]	Diatoms (P2) [mmol N m <sup>-3</sup> ]	Coccolithophorids (P3) [mmol N m <sup>-3</sup> ]	Microzooplankton (Z1) [mmol N m <sup>-3</sup> ]	Mesozooplankton (Z2) [mmol N m <sup>-3</sup> ]
(1) 0.15 (63%)	0.06 (24%)	0.03 (13%)	0.13	0.28
(2) 0.17 (77%)	0.05 (23%)	N/A	0.14	0.31

and dissolution of PIC in the lower layer, so the vertical change was smaller in TAlk than in TCO<sub>2</sub> (solid lines in Fig. 2(G) and (H)). The pCO<sub>2sea</sub> depends on TAlk as well as the temperature, salinity and TCO<sub>2</sub> in the surface water, so it could be estimated more precisely than with previous models that did not explicitly incorporate change of TAlk (e.g. Chai et al., 2002). The pCO<sub>2sea</sub> was 401 [μatm] (Table 3), close to the observed values (e.g. Feely et al., 1997). The pCO<sub>2sea</sub> was much higher than the partial pressure of CO<sub>2</sub> in the atmosphere of 357 [μatm] (Appendix A.1; Chai et al., 2002), suggesting the equatorial Pacific upwelling region as a large CO<sub>2</sub> source to the atmosphere, as the observed.

The modeled net community production was obtained by multiplying the nitrogen changes in the water column by the Redfield stoichiometric ratio of 6.625 (Table 1). The modeled vertical profile of net community production reproduced well the observations (Fig. 3(A)), implying that fixing a phytoplankton carbon:nitrogen ratio is a good assumption in this region. The modeled calcification in the euphotic zone (Fig. 3(B)) was lower than the field data during EqPac Survey II (TT011; in August 1992) in which the measured calcification was considered to be higher than the normal conditions (Balch and Kilpatrick, 1996). The modeled column-integrated ratio of calcification to net community production was 0.06, which lies on a lower end of the observed range from 0.03 to 0.12 during EqPac Survey II (Balch and Kilpatrick, 1996). A higher ratio of the calcification to the net community production could be reproduced by changing a few model parameter values which are relevant to coccolithophorids, such as the maximum specific growth rate of coccolithophorids ( $\mu_{3max}$ ) and the half-saturation constant for NH<sub>4</sub> uptake by coccolithophorids ( $K_{P3\_NH4}$ ), as described in Section 3.2.

The modeled bSiO<sub>2</sub> production with depth showed a pattern similar to that of the net community

Table 3

Model results in the surface water in (I) calcification model simulation and (II) no-calcification model simulations

State variable	(I)	(II)
Picoplankton [mmol N m <sup>-3</sup> ]	0.23	0.36
Diatoms [mmol N m <sup>-3</sup> ]	0.13	0.06
Coccolithophorids [mmol N m <sup>-3</sup> ]	0.06	N/A
Total phytoplankton [mmol N m <sup>-3</sup> ]	0.43	0.42
Microzooplankton [mmol N m <sup>-3</sup> ]	0.35	0.38
Mesozooplankton [mmol N m <sup>-3</sup> ]	0.65	0.89
Total zooplankton [mmol N m <sup>-3</sup> ]	0.99	1.27
NO <sub>3</sub> [mmol N m <sup>-3</sup> ]	6.08	3.56
NH <sub>4</sub> [mmol N m <sup>-3</sup> ]	0.14	0.10
Si(OH) <sub>4</sub> [mmol Si m <sup>-3</sup> ]	3.08	5.30
TAlk [mmol m <sup>-3</sup> ]	2360.9	2383.7
TCO <sub>2</sub> [mmol C m <sup>-3</sup> ]	2045.9	2034.5
pCO <sub>2sea</sub> [μatm]	401.0	353.5
Picoplankton specific growth rate [day <sup>-1</sup> ]	1.01	0.97
Diatom specific growth rate [day <sup>-1</sup> ]	0.45	0.55
Coccolithophorid specific growth rate [day <sup>-1</sup> ]	0.24	N/A
Specific grazing rate on picoplankton by microzooplankton [day <sup>-1</sup> ]	0.95	0.92
Specific grazing rate on diatoms by mesozooplankton [day <sup>-1</sup> ]	0.23	0.30
Specific grazing rate on coccolithophorids by mesozooplankton [day <sup>-1</sup> ]	0.10	N/A
Specific predation rate on microzooplankton by mesozooplankton [day <sup>-1</sup> ]	0.32	0.51
Specific grazing rate on PON by mesozooplankton [day <sup>-1</sup> ]	0.02	0.04

production although the modeled bSiO<sub>2</sub> production decreased more rapidly with depth (Fig. 3(A) and (C)). The modeled vertical profile reproduced the field data (Leynaert et al., 2001), but the model overestimated the field results in the lower layer. Unlike the calcification data, the bSiO<sub>2</sub> data were collected during the EBENE cruise in October–November 1996, which took place during a “neutral scenario” between El Niño and La Niña (Leynaert et al., 2001). Therefore, the bSiO<sub>2</sub> data can be considered to be normal, and the model-data misfit was probably caused by other biological factors such as a vertical change in the diatom

Si:N uptake ratio that was not considered in the present model.

The modeled  $\text{bSiO}_2$ :POC production ratio remarkably decreased with depth, from 0.03 at the surface to nearly zero at 120 m depth, following the rapid decrease in diatom biomass with depth (solid line in Fig. 2(A)) as observed (Barber et al., 1996). The modeled PIC:POC production ratio, by contrast, was relatively similar with depth but had its maximum of 0.07 around 50 m depth (Fig. 3(D)). The increased dominance of coccolithophorids in the subsurface layers resulted from its strategy to seek for  $\text{NH}_4$  which was rapidly consumed by picoplankton in the surface water (solid line in Fig. 2(E)). This implies that the calcification in the subsurface layers, which cannot be detected by satellite observations, plays a considerable role in

significant PIC sedimentation in the equatorial Pacific.

The modeled export flux of PON, POC,  $\text{bSiO}_2$ , and PIC at 120 m depth was  $0.58 \text{ (mmol N m}^{-2} \text{ day}^{-1})$ ,  $3.84 \text{ (mmol C m}^{-2} \text{ day}^{-1})$ ,  $1.46 \text{ (mmol Si m}^{-2} \text{ day}^{-1})$ , and  $0.60 \text{ (mmol C m}^{-2} \text{ day}^{-1})$ , respectively (Table 4). All the export fluxes of PON, POC and  $\text{bSiO}_2$  lie within the observed wide ranges of  $0.38\text{--}4.65 \text{ (mmol N m}^{-2} \text{ day}^{-1})$ ,  $0.6\text{--}20 \text{ (mmol C m}^{-2} \text{ day}^{-1})$  and  $0.05\text{--}3.9 \text{ (mmol Si m}^{-2} \text{ day}^{-1})$ , respectively. The PIC:POC export ratio (rain ratio) in the equatorial Pacific upwelling region was 0.16 in this study (Table 4). This is relatively higher than recent estimates of  $0.05\text{--}0.08$  for the global-mean rain ratio (e.g. Yamanaka and Tajika, 1996; Najjar and Orr, 1998; Milliman et al., 1999; Sarmiento et al., 2002; Fujii et al., 2005), implying notable PIC export in the

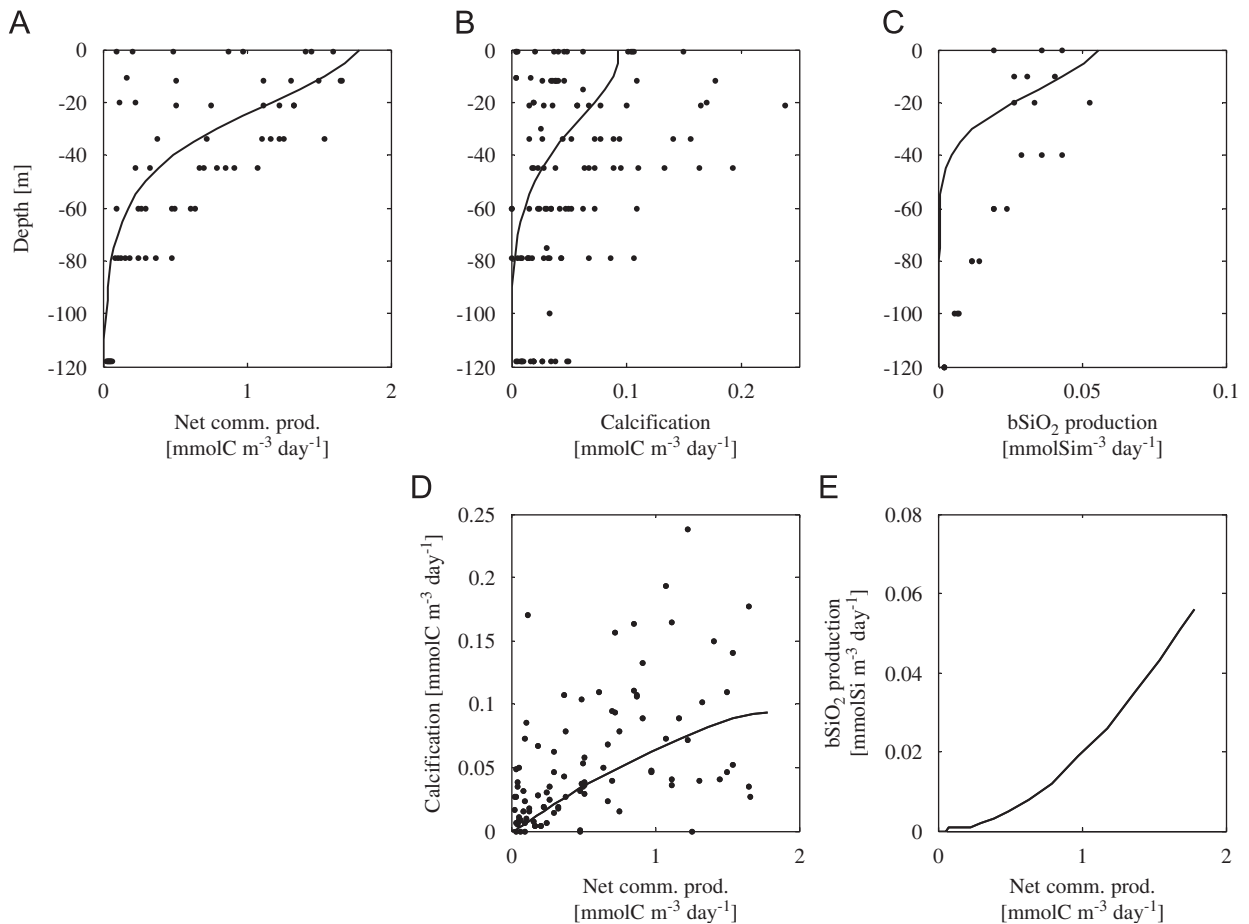


Fig. 3. Modeled (A) vertical profile of net community production ( $\text{mmol C m}^{-3} \text{ day}^{-1}$ ), (B) vertical profile of calcification ( $\text{mmol C m}^{-3} \text{ day}^{-1}$ ), (C) vertical profile of  $\text{bSiO}_2$  production ( $\text{mmol Si m}^{-3} \text{ day}^{-1}$ ), (D) calcification ( $\text{mmol C m}^{-3} \text{ day}^{-1}$ ) vs. net community production ( $\text{mmol C m}^{-3} \text{ day}^{-1}$ ), and (E)  $\text{bSiO}_2$  production ( $\text{mmol Si m}^{-3} \text{ day}^{-1}$ ) vs. net community production ( $\text{mmol C m}^{-3} \text{ day}^{-1}$ ) in the euphotic zone. Dots denote the field observation data from EBENE (Leynaert et al., 2001) for  $\text{bSiO}_2$  production and EqPac Survey II (TT011) (Balch and Kilpatrick, 1996) for the others.

equatorial Pacific compared to the global ocean, as reported by Balch and Kilpatrick (1996).

The modeled  $\text{bSiO}_2$ :PON export ratio was 2.52 (Table 4), which lies between the maximum ratio of nearly 4 obtained by Dugdale et al. (2002) and other sediment trap data of 0.10–1.25 (Dunne et al., 1999). Recent data show that bacterial protease activity accelerates the dissolution of  $\text{bSiO}_2$  in the euphotic zone (Bidle and Azam, 1999), and that such process is strongly dependent on water temperature (Bidle et al., 2002, 2003). Other previous studies suggested that the dissolution of  $\text{bSiO}_2$  is correlated to the percentage of dead diatoms, and that other factors controlling  $\text{bSiO}_2$  dissolution rate besides water temperature, such as differences in organic coatings that protect against  $\text{bSiO}_2$  dissolution between live and dead diatoms, are probably required (Beucher et al., 2004; Fujii and Chai, 2005). These factors, which were not taken into account in the present model, probably contribute to the large spatial and temporal variation among the observed  $\text{bSiO}_2$ :PON export ratios and to regard sedimented biogenic silica under the equatorial upwelling area as an amplifier of changes in surface properties (Dugdale et al., 2002).

### 3.2. Comparison with no-calcification model results

We compared the standard model experimental results with and without coccolithophorids and its calcification processes (hereafter calcification and no-calcification model simulation, respectively). The no-calcification model results were obtained by eliminating all the parameters that are associated with coccolithophorids and its calcification processes and by modifying the grazing preference by mesozooplankton properly (Table 1).

The model results show that surface diatom biomass is less than half in the no-calcification model simulation, although the diatom specific growth rate (diatom growth rate divided by its biomass) is 23% higher due to higher  $\text{Si(OH)}_4$  concentration (Table 3; Fig. 2(A) and (F)). This results from absence of grazing pathway by mesozooplankton on coccolithophorids and subsequently higher grazing pressure on diatoms by mesozooplankton (by a factor of 1.3 in terms of the specific grazing rate, grazing rate divided by prey's biomass) in the no-calcification model simulation (Table 3). The absence of coccolithophorids in the no-calcification model simulation yields enhancement of the other feeding pathways by

Table 4  
Comparison of export fluxes and ratios at the bottom of euphotic zone (120 m depth).

Experiment	PON ( $\text{mmol N m}^{-2}$ $\text{day}^{-1}$ )	POC ( $\text{mmol C m}^{-2}$ $\text{day}^{-1}$ )	$\text{bSiO}_2$ ( $\text{mmol Si m}^{-2}$ $\text{day}^{-1}$ )	PIC ( $\text{mmol C m}^{-2}$ $\text{day}^{-1}$ )	$\text{bSiO}_2$ :PON ratio	PIC:POC ratio	Source
Survey I (TT007)	0.38–0.95	0.6–6.3	0.05–0.1		0.29–0.34		(1),(2), (3),(4)
Time series I (TT008)		1.9–5					(5),(6)
Survey II (TT011)	0.6–4.65	1.5–19.5	0.4–3.9		0.79–1.25		(1),(2), (3),(4)
Time series II (TT012)		2.4					(6)
FLUPAC	$2.90 \pm 0.65$	$17.0 \pm 2.5$		$2.3 \pm 0.3$	0.10–0.23		(7),(8), (3),(4)
OLIPAC	0.68	7.1					(9),(3), (4)
Zonal Flux					0.14–0.45		(3)
EBENE		9–20	2.6				(10),(11)
Model	1.36–1.39	3.8–5.4					(12),(4)
Model	0.76	5.01	2.36	N/A	3.11	N/A	(13)
Model	0.69–0.98	5.04–7.15	0.35–3.20	N/A	0.36–4.64	N/A	(4)
Model (calcification model simulation)	0.58	3.84	1.46	0.60	2.52	0.16	This study
Model (no-calcification model simulation)	0.51	3.38	0.74	N/A	1.45	N/A	This study

Sources: (1) Luo et al. (1995); (2) Murray et al. (1996); (3) Dunne et al. (1999); (4) Dugdale et al. (2002); (5) Buesseler et al. (1995); (6) Bacon et al. (1996); (7) Le Borgne et al. (1995); (8) Rodier and Le Borgne (1997); (9) Rainbault et al. (1999); (10) Le Borgne et al. (1998); (11) Leynaert et al. (2001); (12) Loukos et al. (1997); (13) Dugdale and Wilkerson (1998).

mesozooplankton, namely predation on microzooplankton and grazing on PON as well, by a factor of 1.6 and 1.8, respectively (Table 3). As a result, mesozooplankton biomass is 26% higher in the no-calcification model simulation (Table 3; Fig. 2(C)). The substantially enhanced predation on microzooplankton by mesozooplankton in the no-calcification model simulation slightly lowers grazing pressure on picoplankton by microzooplankton, which leads to 33% higher picoplankton biomass regardless of its lower specific growth rate due to lower  $\text{NH}_4$  and  $\text{NO}_3$  concentrations than in the calcification model simulation (Table 3; Fig. 2(A), (D) and (E)).

Compared to the change in each phytoplankton biomass between the calcification and no-calcification model simulations, the total phytoplankton biomass in the surface water is similar between the two models, because the absence of coccolithophorids and the lower diatom biomass in the no-calcification model simulation is partly compensated by the higher picoplankton biomass (Table 3; Fig. 2(A) and (B)). The export flux of PON or POC, which is generated from phytoplankton mortality and fecal pellet, is similar as well (changing only by 12%; Table 4). On the other hand, the  $\text{bSiO}_2$  export is lower in the no-calcification model simulation by 49% (Table 4). Same as the relationship between the surface  $\text{NO}_3$  and  $\text{Si(OH)}_4$ , the change is relatively smaller in surface  $\text{TCO}_2$  than in TALK between the two models (Table 3; Fig. 2(G) and (H)). The higher TALK and lower  $\text{TCO}_2$  cause lower  $\text{pCO}_{2\text{sea}}$  in the no-calcification model simulation by 47  $\mu\text{atm}$  (Table 3), which is primarily affected by the increase in TALK.

## 4. Discussion

### 4.1. Sensitivity to biogeochemical parameters (Experiment 1)

We tested model sensitivity to each biogeochemical parameter by changing the parameter value from 0.5 to 1.5 times the standard value (Table 1). We found the model results, i.e., surface plankton abundance, concentrations of nutrients, TALK and  $\text{TCO}_2$ ,  $\text{pCO}_{2\text{sea}}$ , and export fluxes of PON,  $\text{bSiO}_2$  and PIC, are especially sensitive to changes in six model parameters relevant to grazing or predation by zooplankton, namely the maximum grazing and/or predation rates by zooplankton ( $G1_{\text{max}}$  and  $G2_{\text{max}}$ ), the half-saturation constants for zooplank-

ton ingestion ( $K1_{\text{gr}}$  and  $K2_{\text{gr}}$ ), the mesozooplankton excretion rate to  $\text{NH}_4$  ( $\text{reg}_2$ ), and the mesozooplankton specific mortality rate ( $\gamma_2$ ) (Table 5). This suggests that the phytoplankton in the equatorial Pacific upwelling area is universally and severely exposed under the top-down (grazing) control by zooplankton. This is consistent with the observed results that grazing has been invoked as the control on loss rates (Walsh, 1976; Landry et al., 1997; Dugdale et al., 2002).

The maximum grazing or predation rate by mesozooplankton ( $G2_{\text{max}}$ ) is the most significant parameter to determine surface diatoms, coccolithophorids,  $\text{Si(OH)}_4$ , TALK,  $\text{TCO}_2$ , and export fluxes of PON and PIC (Table 5; Fig. 4). The lower  $G2_{\text{max}}$  causes lower grazing pressure on diatoms and coccolithophorids and subsequently higher diatom and coccolithophorid biomass, which leads to higher export fluxes of POC,  $\text{bSiO}_2$  and PIC, and lower TALK and  $\text{TCO}_2$  (Fig. 4(A)–(F)). The simultaneous decrease in TALK and  $\text{TCO}_2$  (238 ( $\text{mmol m}^{-3}$ ) and 149 ( $\text{mmol C m}^{-3}$ ), respectively) with  $G2_{\text{max}}$  decrease compensates each other in terms of  $\text{pCO}_{2\text{sea}}$  change, which yields  $\text{pCO}_{2\text{sea}}$  decrease of 137 [ $\mu\text{atm}$ ] (Fig. 4(E)), significant but relatively small compared to the individual changes in TALK and  $\text{TCO}_2$ .

The maximum grazing rate on picoplankton by microzooplankton ( $G1_{\text{max}}$ ) is the most effective parameter in determining surface picoplankton biomass and  $\text{NO}_3$  (Table 5). Two phytoplankton-related parameters (the initial slope of  $P$ – $I$  curve ( $\alpha$ ) and the maximum specific growth rate of picoplankton ( $\mu_{1\text{max}}$ ) also control the model results, but less broadly than the zooplankton-related parameters above do (Table 5). The surface TALK and  $\text{TCO}_2$  vary by 21–45 ( $\text{mmol m}^{-3}$ ) and 53–81 ( $\text{mmol C m}^{-3}$ ), respectively, by changing one of the three parameter values (Table 5; Fig. 5(A) and (B)). These changes are relatively small compared to those brought by  $G2_{\text{max}}$  change of 238 ( $\text{mmol m}^{-3}$ ) and 149 ( $\text{mmol C m}^{-3}$ ), respectively. However, surface TALK and  $\text{TCO}_2$  change in a different way with parameter values, i.e. surface TALK increases and  $\text{TCO}_2$  decreases with parameter values of  $\alpha$  and  $\mu_{1\text{max}}$ , and vice versa for  $G1_{\text{max}}$ . This is the reason why the  $\text{pCO}_{2\text{sea}}$  change by changing these parameter values is relatively large (184, 147 and 160 [ $\mu\text{atm}$ ] for  $\alpha$ ,  $\mu_{1\text{max}}$  and  $G1_{\text{max}}$ , respectively; Table 5; Fig. 5(C)).

The surface coccolithophorid biomass and the export PIC flux at 120 m depth are sensitive to

Table 5

Sensitivity of surface phytoplankton ( $P1$ ,  $P2$  and  $P3$  [ $\text{mmol N m}^{-3}$ ]), zooplankton ( $Z1$  and  $Z2$  [ $\text{mmol N m}^{-3}$ ]), nutrients ( $\text{NO}_3$  [ $\text{mmol N m}^{-3}$ ],  $\text{NH}_4$  [ $\text{mmol N m}^{-3}$ ] and  $\text{Si(OH)}_4$  [ $\text{mmol Si m}^{-3}$ ]), TALK [ $\text{mmol m}^{-3}$ ],  $\text{TCO}_2$  [ $\text{mmol C m}^{-3}$ ] and  $\text{pCO}_{2\text{sea}}$  [ $\mu\text{atm}$ ] and of export PON [ $\text{mmol N m}^{-2} \text{day}^{-1}$ ],  $\text{bSiO}_2$  [ $\text{mmol Si m}^{-2} \text{day}^{-1}$ ] and PIC [ $\text{mmol C m}^{-2} \text{day}^{-1}$ ] fluxes, to biogeochemical parameters in calcification model

Parameter	$P1$ (0.23)	$P2$ (0.13)	$P3$ (0.06)	$Z1$ (0.35)	$Z2$ (0.65)	$\text{NO}_3$ (6.08)	$\text{NH}_4$ (0.14)	$\text{Si(OH)}_4$ (3.08)	TALK (2360.9)	$\text{TCO}_2$ (2045.9)	$\text{pCO}_{2\text{sea}}$ (401.02)	PON (0.58)	$\text{bSiO}_2$ (1.36)	PIC (0.60)
$\alpha$	<b>0.24</b>	0.08	<b>0.08</b>	0.17	<b>0.75</b>	<b>7.84</b>	0.08	0.53	21.39	80.91	<b>183.84</b>	0.19	0.16	0.46
$\mu_{1\text{max}}$	0.20	0.08	<b>0.08</b>	0.21	<b>0.66</b>	<b>6.49</b>	0.08	1.90	33.12	52.64	<b>147.05</b>	0.03	0.59	<b>0.84</b>
$\Psi$	0.10	0.03	0.02	0.10	0.41	4.78	0.03	0.72	9.55	56.89	<b>86.66</b>	0.13	0.23	0.41
$K_{\text{NO}_3}$	0.03	0.01	0.01	0.02	0.08	0.75	0.00	0.23	3.83	5.83	16.53	0.00	0.07	0.10
$K_{\text{NH}_4}$	0.17	0.05	0.04	0.10	0.50	5.53	0.10	1.50	18.69	47.19	<b>108.01</b>	0.05	0.48	0.42
$\mu_{2\text{max}}$	0.09	0.09	0.02	0.01	0.15	1.31	0.03	<b>3.22</b>	6.92	10.22	26.92	0.04	0.97	0.19
$K_{\text{Si(OH)}_4}$	0.02	0.04	0.00	0.01	0.01	0.32	0.01	2.03	0.84	1.33	3.83	0.05	0.63	0.02
$K_{\text{S}_2\text{NH}_4}$	0.01	0.01	0.01	0.01	0.02	0.16	0.04	0.38	5.20	1.53	5.00	0.02	0.12	0.16
$W_1$	0.00	0.02	0.00	0.00	0.01	0.02	0.00	0.15	0.13	0.24	0.65	0.03	0.03	0.01
$\mu_{3\text{max}}$	0.15	0.06	<b>0.11</b>	0.02	0.32	3.18	0.04	1.44	46.51	14.33	<b>67.20</b>	0.09	0.45	<b>1.37</b>
$K_{\text{S}_3\text{NO}_3}$	0.02	0.00	0.01	0.00	0.03	0.22	0.01	0.15	5.52	0.92	6.62	0.01	0.05	0.16
$K_{\text{S}_3\text{NH}_4}$	0.06	0.02	<b>0.07</b>	0.03	0.11	0.71	0.01	0.57	35.24	15.30	26.28	0.09	0.18	<b>1.08</b>
$W_3$	0.02	0.01	0.02	0.00	0.03	0.29	0.01	0.17	4.55	0.25	7.00	0.01	0.06	0.18
$G_{1\text{max}}$	<b>2.04</b>	<b>0.15</b>	<b>0.11</b>	0.16	<b>0.70</b>	<b>8.20</b>	<b>0.16</b>	<b>3.84</b>	45.39	55.90	<b>160.23</b>	0.34	<b>1.37</b>	<b>1.14</b>
$K_{1\text{gr}}$	<b>0.43</b>	0.09	<b>0.11</b>	0.22	<b>0.72</b>	<b>7.62</b>	0.09	2.54	43.93	58.95	<b>174.41</b>	0.04	0.81	<b>1.13</b>
$\text{reg}_1$	0.21	0.03	0.04	0.08	0.29	2.79	0.01	1.01	17.43	46.01	<b>112.43</b>	0.02	0.33	0.46
$G_{2\text{max}}$	<b>1.02</b>	<b>0.45</b>	<b>1.12</b>	0.21	<b>0.71</b>	<b>7.23</b>	<b>0.15</b>	<b>5.95</b>	237.68	148.84	<b>137.18</b>	<b>1.74</b>	<b>1.75</b>	<b>7.25</b>
$K_{2\text{gr}}$	<b>1.19</b>	<b>0.23</b>	<b>0.22</b>	0.31	<b>0.92</b>	<b>7.15</b>	<b>0.85</b>	<b>5.75</b>	72.74	36.60	<b>138.33</b>	<b>0.76</b>	<b>1.82</b>	<b>2.04</b>
$\gamma_3$	0.02	0.02	0.00	0.01	0.02	0.19	0.01	0.57	1.21	2.62	6.66	0.03	0.16	0.04
$\gamma_6$	0.05	0.02	0.05	0.02	0.12	0.93	0.01	0.53	15.21	2.43	25.48	0.01	0.17	0.42
$\gamma_2$	<b>0.48</b>	0.12	<b>0.09</b>	0.06	<b>1.01</b>	<b>6.13</b>	0.09	<b>3.57</b>	36.12	55.47	<b>135.07</b>	0.15	1.10	<b>0.92</b>
$\text{reg}_2$	<b>0.51</b>	<b>0.23</b>	<b>0.26</b>	0.18	<b>0.77</b>	<b>7.51</b>	<b>0.15</b>	<b>5.08</b>	85.02	33.55	<b>114.90</b>	<b>0.59</b>	<b>1.56</b>	<b>2.42</b>
$\gamma_7$	0.00	0.00	0.00	0.00	0.00	1.59	0.01	0.06	1.32	0.78	0.58	0.46	0.02	0.01
$\gamma_4$	0.01	0.03	0.00	0.00	0.00	0.15	0.01	0.68	0.30	0.57	1.32	0.02	0.18	0.02
$\gamma_8$	0.00	0.00	0.00	0.00	0.00	0.00	0.00	0.00	1.00	0.64	0.30	0.00	0.00	0.14
$W_2$	0.01	0.00	0.00	0.00	0.04	1.39	0.02	0.02	0.72	1.22	3.05	0.19	0.00	0.06
$W_4$	0.02	0.04	0.00	0.01	0.02	0.38	0.01	1.14	0.94	1.88	4.76	0.03	1.22	0.02
$W_5$	0.00	0.00	0.00	0.00	0.00	0.00	0.00	0.00	1.28	0.83	0.40	0.00	0.00	0.48
$R_{\text{SiN}}$	0.08	<b>0.16</b>	0.01	0.03	0.19	2.70	0.05	2.97	8.60	15.19	38.69	0.17	0.92	0.17
$\gamma_5$	0.00	0.00	0.00	0.00	0.00	0.01	0.02	0.02	1.78	1.21	0.53	0.00	0.01	0.05

Values in parentheses denote model results in the standard experiment. The other values mean difference by changing each parameter value from 0.5 to 1.5 times the standard parameter value. The values in bold letters are those that exceed 100% of each model compartment concentration (10% of those for TALK,  $\text{TCO}_2$ , and  $\text{pCO}_{2\text{sea}}$ ). The parameters in bold letters strongly affect the model results and are described in Section 4.1.

many parameters (Table 5). For example, a few parameters like the maximum specific growth rates of coccolithophorids ( $\mu_{3\text{max}}$ ) and the half-saturation constant for  $\text{NH}_4$  uptake by coccolithophorids ( $K_{P3\text{NH}_4}$ ) specialize to control the two model state variables. This means that the modeled coccolithophorids and PIC could change in a sensitive and complicated way with a narrow range of the parameter values. For more realistic simulation of carbon cycling in this region, we need further field data, especially for vertical profiles of POC, PIC, coccolithophorid biomass

and its composition ratio for the phytoplankton community.

The model sensitivity study to the five parameters of  $\alpha$ ,  $\mu_{1\text{max}}$ ,  $\mu_{3\text{max}}$ ,  $G_{1\text{max}}$  and  $G_{2\text{max}}$  reveals that the  $\text{bSiO}_2$ :PON export ratio and the PIC:POC export ratio (rain ratio) at 120 m depth could vary by 0.40–2.83 and 0.00–0.56, respectively (Fig. 6). Considering that the observation-based estimates of the global rain ratio vary from 0.05 to 0.25 (e.g. Fujii et al., 2005) and excluding the model results in which the rain ratio was out of the range (Fig. 6(B)), we obtained a range of 1.51–2.75 for the  $\text{bSiO}_2$ :PON export ratio (Fig. 6(A)).

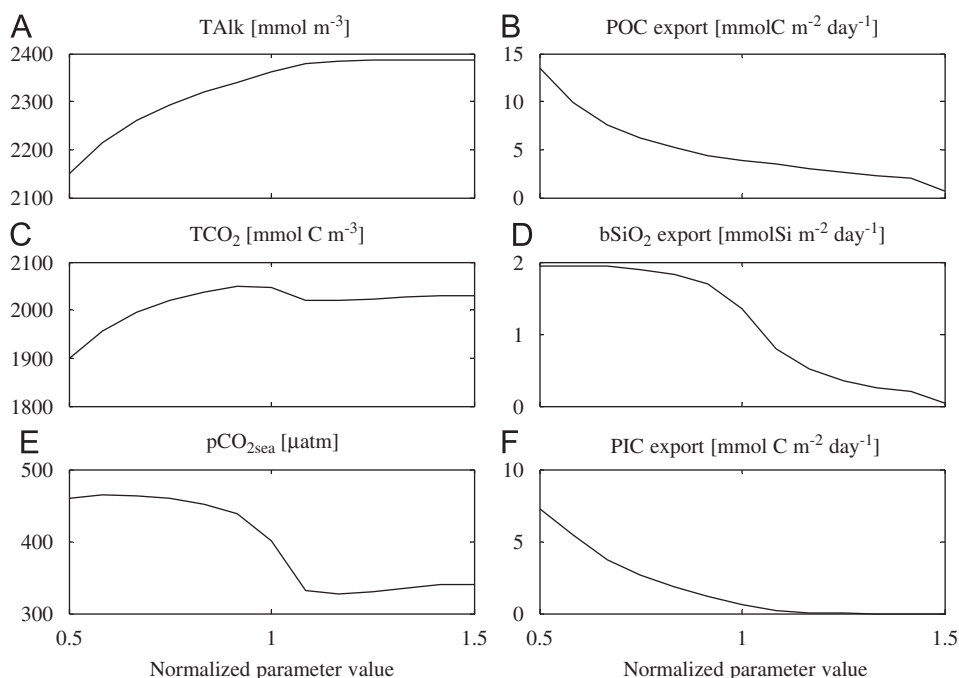


Fig. 4. Modeled (A) surface TALK ( $\text{mmol m}^{-3}$ ), (B) export POC flux ( $\text{mmol C m}^{-2} \text{ day}^{-1}$ ) at 120 m depth, (C) surface  $\text{TCO}_2$  ( $\text{mmol C m}^{-3}$ ), (D) export  $\text{bSiO}_2$  flux ( $\text{mmol Si m}^{-2} \text{ day}^{-1}$ ) at 120 m depth, (E)  $\text{pCO}_{2\text{sea}}$  [ $\mu\text{atm}$ ], and (F) export PIC flux at 120 m depth ( $\text{mmol C m}^{-2} \text{ day}^{-1}$ ), obtained by changing the maximum grazing or predation rate by mesozooplankton ( $G_{2\text{max}}$ ) from 0.5 to 1.5 times the standard value.

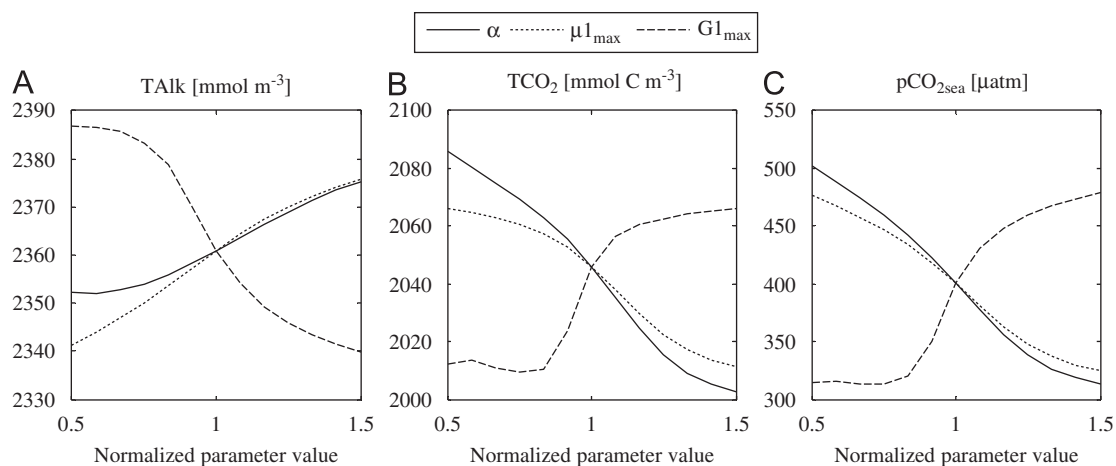


Fig. 5. Modeled (A) surface TALK ( $\text{mmol m}^{-3}$ ), (B) surface  $\text{TCO}_2$  ( $\text{mmol C m}^{-3}$ ), and (C)  $\text{pCO}_{2\text{sea}}$  [ $\mu\text{atm}$ ], obtained by changing the initial slope of  $P-I$  curve ( $\alpha$ ), the maximum specific growth rates of picoplankton ( $\mu_{1\text{max}}$ ), and the maximum specific grazing rate on picoplankton by mesozooplankton ( $G_{1\text{max}}$ ) from 0.5 to 1.5 times the standard value.

#### 4.2. Sensitivity to source $\text{Si}(\text{OH})_4$ concentration (Experiment 2)

Experiment 2 is similar to the experiment conducted by Dugdale et al. (2002), i.e. the source (120 m

depth)  $\text{Si}(\text{OH})_4$  concentration was varied from 3.0 to 15.0 ( $\text{mmol Si m}^{-3}$ ), corresponding to the full range of JGOFS equatorial values of 3–13 ( $\text{mmol Si m}^{-3}$ ) (Dugdale et al., 2002). The  $\text{NO}_3$  concentration at 120 m depth was held constant at 12.0 ( $\text{mmol N m}^{-3}$ ).

#### 4.2.1. Calcification model simulation

With source (120 m depth)  $\text{Si}(\text{OH})_4$  concentration increases, surface  $\text{Si}(\text{OH})_4$  concentration increases linearly from 1.8 to 6.6 ( $\text{mmol Si m}^{-3}$ ) (solid line in Fig. 7(F)). The surface  $\text{Si}(\text{OH})_4$  increase enhances surface diatom growth (Fig. 8(B)) and increases surface diatom biomass by a factor of 4.3 (solid green line in Fig. 7(A)). The surface diatom increase results in a remarkable switch in feeding by mesozooplankton from microzooplankton to diatoms as the source  $\text{Si}(\text{OH})_4$  increases (Fig. 8(B) and (D)). The declined predation on microzooplankton by mesozooplankton enhances grazing pressure on picoplankton by microzooplankton (Fig. 8(A)), causing a decrease in surface picoplankton biomass with source  $\text{Si}(\text{OH})_4$  increase (solid line in Fig. 7(A)). The decrease in surface picoplankton biomass is more rapid with lower source  $\text{Si}(\text{OH})_4$  concentrations.

The surface diatom increase with source  $\text{Si}(\text{OH})_4$  concentration also yields a slight switch in grazing by mesozooplankton from coccolithophorids to diatoms (Fig. 8(B) and (C)), which increases surface coccolithophorid biomass (Fig. 7(B)). The surface coccolithophorid biomass has its maximum at source  $\text{Si}(\text{OH})_4 = 8\text{--}9$  ( $\text{mmol Si m}^{-3}$ ) and then decreases with higher source  $\text{Si}(\text{OH})_4$  concentrations due to slight  $\text{NO}_3$  regulation on the coccolithophorid growth as the result of higher diatom growth (solid lines in Figs. 7(B), (E), 8(B) and (C)).

The total phytoplankton biomass in the surface water has its minimum at source  $\text{Si}(\text{OH})_4 = 5$  ( $\text{mmol Si m}^{-3}$ ) (solid line in Fig. 7(C)). The phytoplankton composition ratio in the surface water is 80%, 11%, and 9% at source  $\text{Si}(\text{OH})_4 = 3$  ( $\text{mmol Si m}^{-3}$ ); 52%, 33%, and 15% at source  $\text{Si}(\text{OH})_4 = 7.5$  ( $\text{mmol Si m}^{-3}$ ); and 46%, 42%, and 12% at source  $\text{Si}(\text{OH})_4 = 15$  ( $\text{mmol Si m}^{-3}$ ) (solid lines in Fig. 7(D)), indicating substantial increase in diatoms and decrease in picoplankton and relatively similar coccolithophorid biomass with source  $\text{Si}(\text{OH})_4$  increase.

Surface TALK is taken up by the coccolithophorids' calcification process. Hence, TALK has its minimum with source  $\text{Si}(\text{OH})_4 = 7\text{--}8$  ( $\text{mmol Si m}^{-3}$ ) at which surface coccolithophorids biomass had its maximum (solid lines in Fig. 7(B) and (G)). The surface  $\text{TCO}_2$ , which is taken up by both phytoplankton growth and calcification, has its maximum with source  $\text{Si}(\text{OH})_4 = 7$  ( $\text{mmol Si m}^{-3}$ ), mainly as the result of the lowest total phytoplankton biomass in the surface water (solid line in Fig. 7(C) and (H)). The  $\text{pCO}_{2\text{sea}}$  decreases with TALK increase and increases with  $\text{TCO}_2$  increase. The two opposite changes in the  $\text{pCO}_{2\text{sea}}$  by TALK and  $\text{TCO}_2$  varies formed a maximum  $\text{pCO}_{2\text{sea}}$  with source  $\text{Si}(\text{OH})_4 = 7$  ( $\text{mmol Si m}^{-3}$ ) (solid line in Fig. 7(I)). The  $\text{pCO}_{2\text{sea}}$  changes from 357 to 401 [ $\mu\text{atm}$ ], in a similar range as observed (e.g., Feely et al., 1997).

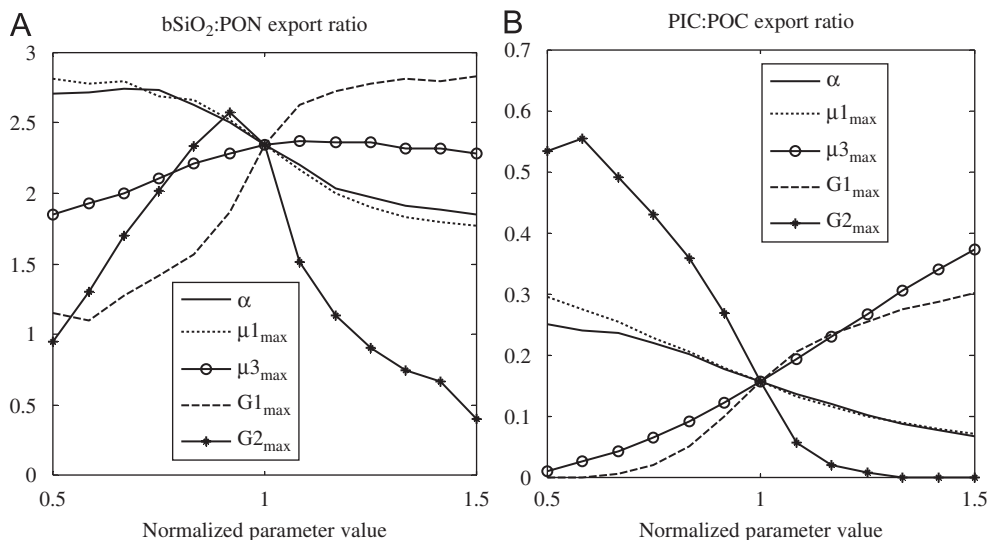


Fig. 6. Modeled (A)  $\text{bSiO}_2\text{:PON}$  export ratio and (B) PIC:POC export ratio (rain ratio) at 120 m depth, obtained by changing the initial slope of  $P\text{--}I$  curve ( $\alpha$ ), the maximum specific growth rates of picoplankton ( $\mu_{1\text{max}}$ ) and coccolithophorids ( $\mu_{3\text{max}}$ ), the maximum specific grazing or predation rates by mesozooplankton ( $G_{1\text{max}}$ ) and mesozooplankton ( $G_{2\text{max}}$ ) from 0.5 to 1.5 times the standard values.

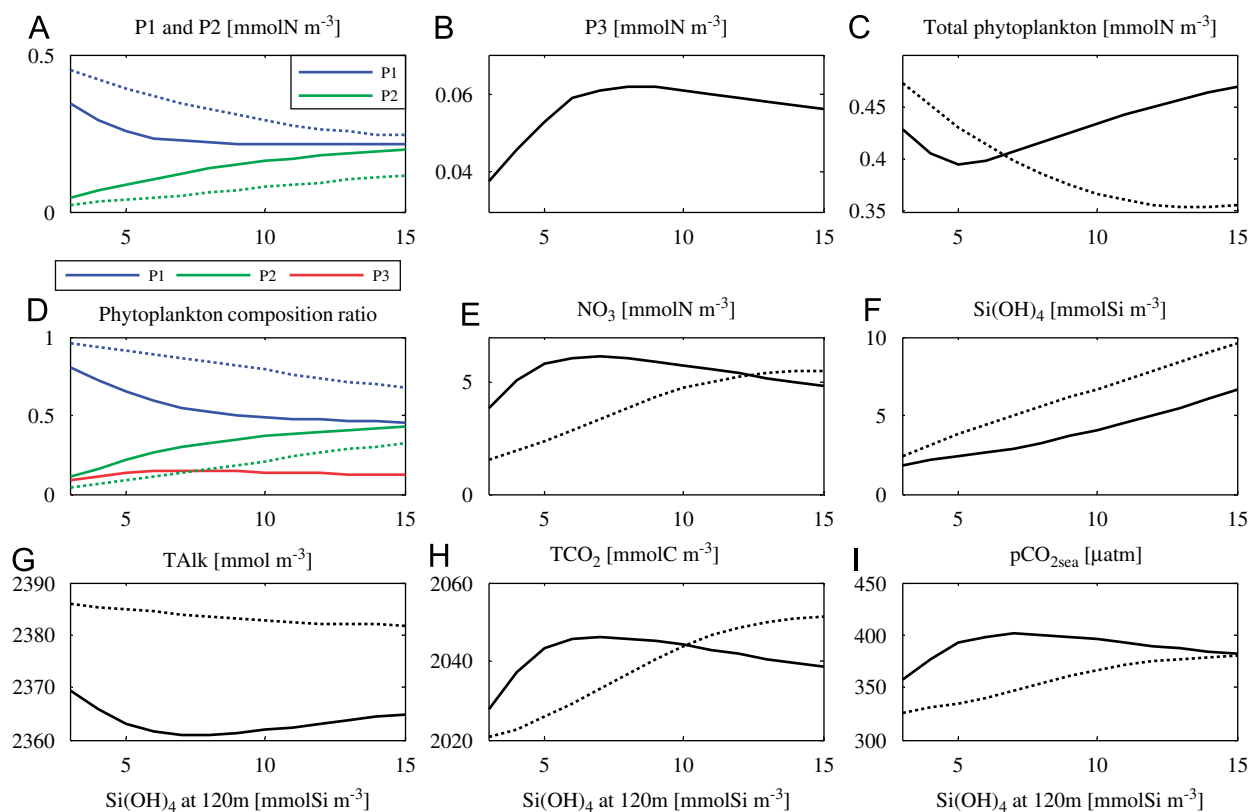


Fig. 7. Modeled surface (A) picoplankton ( $P1$ ; in blue) and diatom ( $P2$ ; in green) ( $\text{mmol N m}^{-3}$ ), (B) coccolithophorids ( $P3$ ) ( $\text{mmol N m}^{-3}$ ), (C) total phytoplankton ( $P1 + P2 + P3$  for calcification model simulation and  $P1 + P2$  for no-calcification model simulation) ( $\text{mmol N m}^{-3}$ ), (D) phytoplankton composition ratio of picoplankton (in blue), diatoms (in green), and coccolithophorids (in red) to total phytoplankton, (E)  $\text{NO}_3$  ( $\text{mmol N m}^{-3}$ ), (F)  $\text{Si(OH)}_4$  ( $\text{mmol Si m}^{-3}$ ), (G) TALK ( $\text{mmol m}^{-3}$ ), (H)  $\text{TCO}_2$  ( $\text{mmol C m}^{-3}$ ), and (I)  $\text{pCO}_{2\text{sea}}$  [ $\mu\text{atm}$ ], vs. source  $\text{Si(OH)}_4$  concentration ( $\text{mmol Si m}^{-3}$ ) in Experiment 2. Solid lines: calcification model results. Dotted lines: no-calcification model results.

With source  $\text{Si(OH)}_4$  increase, or with surface diatom biomass increase, the modeled  $\text{bSiO}_2$  export at 120 m depth dramatically increases by a factor of 6.6 from 0.38 to 2.52 ( $\text{mmol Si m}^{-2} \text{ day}^{-1}$ ) (solid line in Fig. 9(A)). The modeled PON or POC export at 120 m depth also increases with source  $\text{Si(OH)}_4$  concentrations, but only slightly by a factor of 1.2. The modeled PIC export at 120 m depth changes by a factor of 1.6 from 0.38 to 0.60 ( $\text{mmol C m}^{-2} \text{ day}^{-1}$ ) and has its maximum around the standard source  $\text{Si(OH)}_4$  concentration of 7.5 ( $\text{mmol Si m}^{-3}$ ) (Fig. 9(B)). The difference in the curve among PON or POC,  $\text{bSiO}_2$ , and PIC appears because PON or POC is produced by fecal pellet and phytoplankton mortality, while  $\text{bSiO}_2$  and PIC are only produced by diatoms and coccolithophorids, respectively. The modeled  $\text{bSiO}_2$ :PON export ratio at 120 m depth changes by a factor of 5.6, from 0.7 to 3.9 with source  $\text{Si(OH)}_4$  concentrations (solid

line in Fig. 9(C)). The larger extent of change in  $\text{bSiO}_2$  export with source  $\text{Si(OH)}_4$  concentrations (solid line in Fig. 9(A)) than of surface diatom biomass (by a factor of 4.3; solid line in Fig. 7(A)) suggests sedimented detritus under the equatorial Pacific upwelling region act as an amplifier of changes in surface properties (Dugdale et al., 2002). The modeled PIC:POC export ratio (rain ratio) at 120 m depth changes by a factor of 1.5 from 0.11 to 0.16, and its maximum appears at source  $\text{Si(OH)}_4 = 7$ , close to the standard concentration of 7.5 ( $\text{mmol Si m}^{-3}$ ) (Fig. 9(D)).

The model results show that  $\text{pCO}_{2\text{sea}}$  and export PIC:POC and  $\text{bSiO}_2$ :PON ratios, all of which are excellent indices for assessing abilities of  $\text{CO}_2$  release to the atmosphere and detritus sedimentations in the equatorial Pacific, are sensitive to source  $\text{Si(OH)}_4$  concentrations. In particular, the carbonate system in the surface water, PIC export, and the

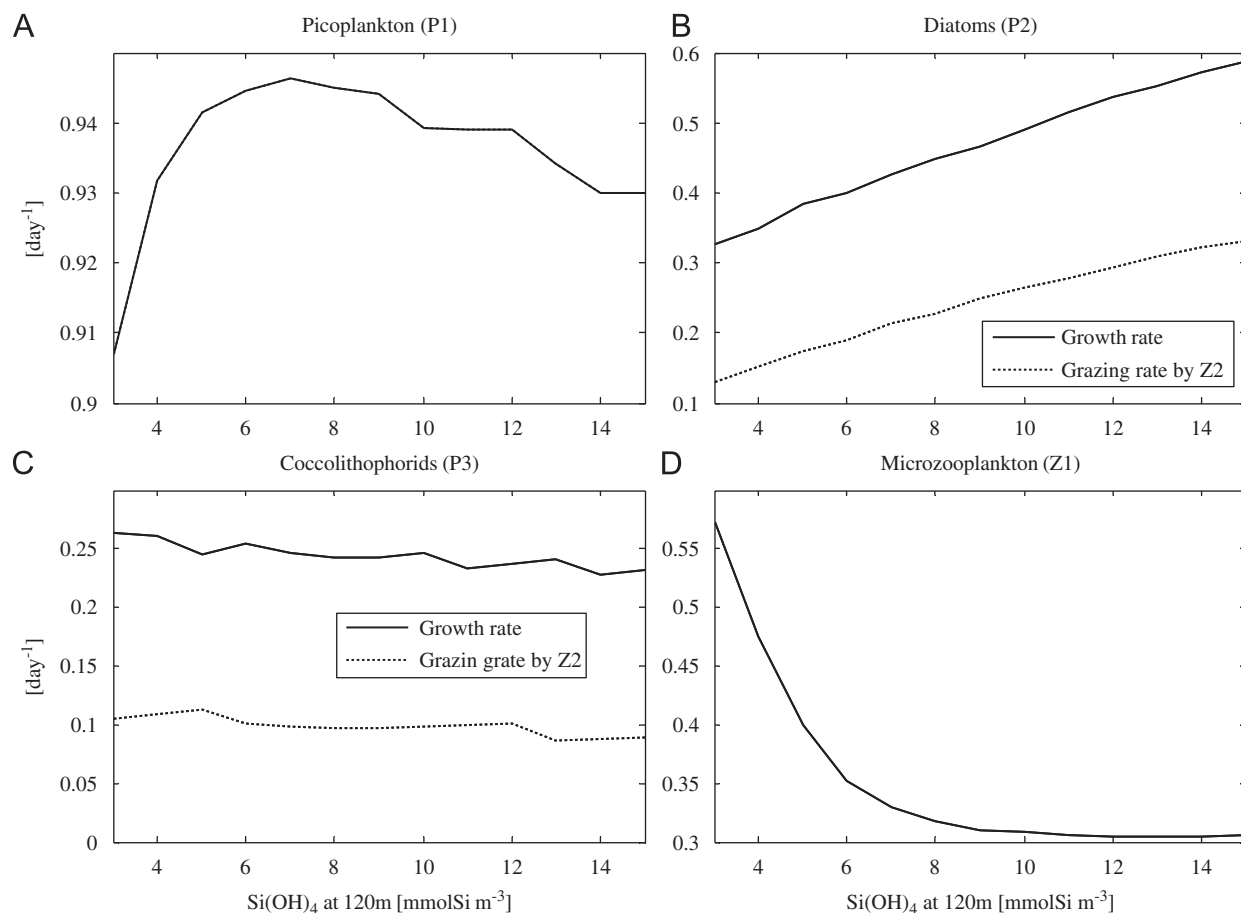


Fig. 8. Modeled specific (divided by each biomass) (A) grazing rate on picoplankton (P1) by microzooplankton (Z1) [ $\text{day}^{-1}$ ], (B) diatom (P2) growth rate and grazing rate by mesozooplankton (Z2) [ $\text{day}^{-1}$ ], (C) coccolithophorid (P3) growth rate and grazing rate by mesozooplankton [ $\text{day}^{-1}$ ], and (D) predation rate on microzooplankton by mesozooplankton [ $\text{day}^{-1}$ ] in the surface water, vs. source  $\text{Si(OH)}_4$  concentration ( $\text{mmolSi m}^{-3}$ ) in Experiment 2.

rain ratio at 120m depth have their peaks near the standard source  $\text{Si(OH)}_4$  concentration of 7.5 ( $\text{mmolSi m}^{-3}$ ), suggesting sensitive change in the  $\text{CO}_2$  release to the atmosphere within a narrow range of the source  $\text{Si(OH)}_4$  concentrations, presumably caused by the physical forcing in the equatorial Pacific upwelling region.

#### 4.2.2. Comparison with no-calcification model results

By eliminating coccolithophorids in the no-calcification model simulation, grazing on diatoms by mesozooplankton is elevated to compensate the missing grazing pathway from coccolithophorids to mesozooplankton (Fig. 10(B)). Therefore, the diatom biomass is lower and the  $\text{Si(OH)}_4$  concentration is higher in the no-calcification model simulation (Fig. 7(A) and (F)). For the same reason, the predation on microzooplankton by mesozoo-

plankton is elevated in the no-calcification model simulation (Fig. 10(C)). The greater predation on microzooplankton by mesozooplankton alleviates grazing pressure on picoplankton by microzooplankton (Fig. 10(A)), which yields higher surface picoplankton biomass with lower source  $\text{Si(OH)}_4$  concentrations in the no-calcification model simulation (Fig. 7(A)). As the source  $\text{Si(OH)}_4$  concentration increases, the surface diatom biomass increases, which leads to dominant mesozooplankton's grazing on diatoms over predation on microzooplankton, in both models (Figs. 7(A), 10(B) and (C)). But the amplitude of decrease in predation on microzooplankton with source  $\text{Si(OH)}_4$  concentrations is greater in the no-calcification model simulation (Fig. 10(C)), which yields greater amplitude of increase in grazing on picoplankton by microzooplankton and decrease in the surface picoplankton

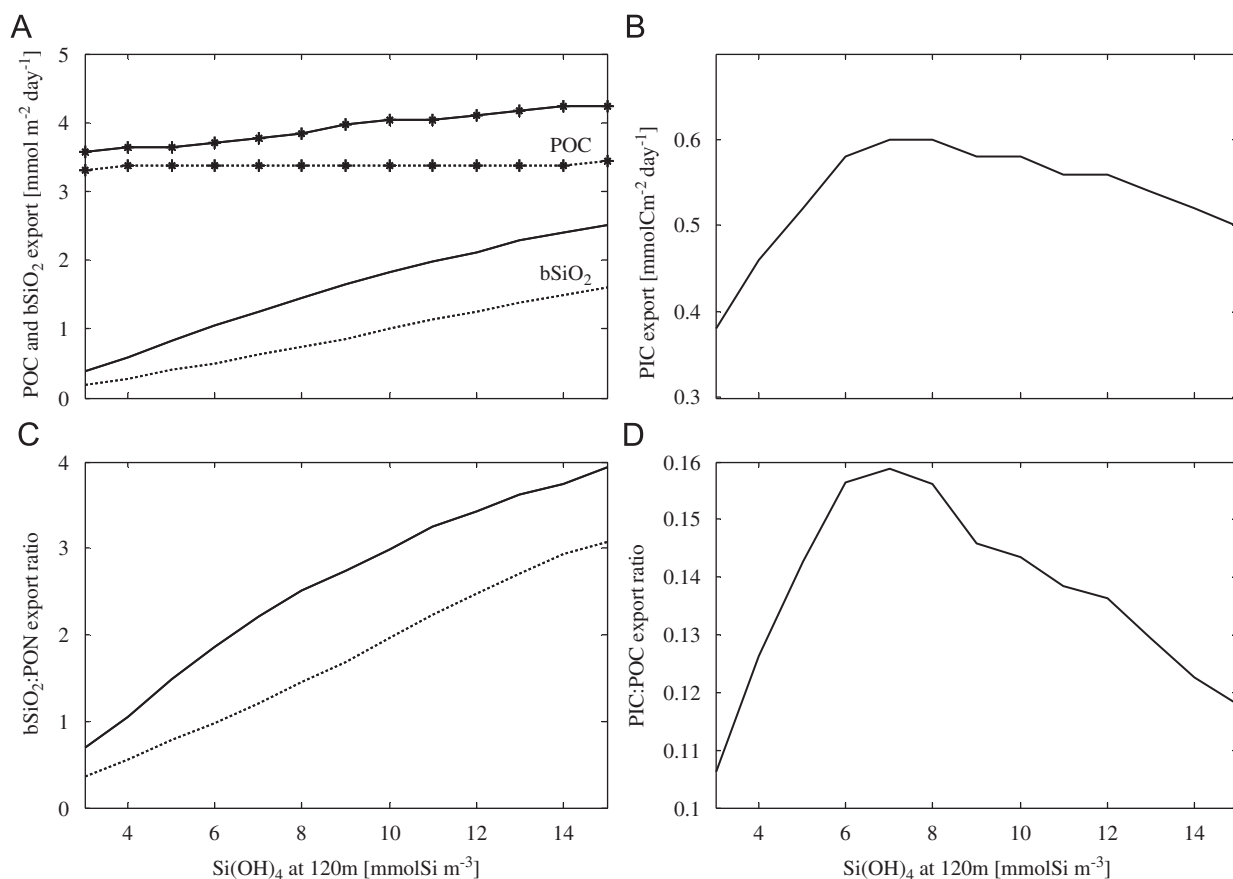


Fig. 9. Modeled (A) export flux of POC ( $\text{mmol C m}^{-2} \text{ day}^{-1}$ ) and  $\text{bSiO}_2$  ( $\text{mmol Si m}^{-2} \text{ day}^{-1}$ ), (B) export PIC flux ( $\text{mmol C m}^{-2} \text{ day}^{-1}$ ), (C) export  $\text{bSiO}_2$ :PON ratio, and (D) export PIC:POC ratio (rain ratio) at 120 m depth vs. source  $\text{Si(OH)}_4$  concentration ( $\text{mmol Si m}^{-3}$ ) in Experiment 2. Solid lines: calcification model results. Dotted lines: no-calcification model results.

biomass (Figs. 7(A) and 10(A)) than in the calcification model simulation. The surface diatom biomass is constantly lower in the no-calcification model simulation because of substantially higher grazing pressure by mesozooplankton than seen in the calcification model simulation (Figs. 7(A) and 10(B)).

The total phytoplankton biomass in the surface water decreases with source  $\text{Si(OH)}_4$  increase in the no-calcification model simulation (dotted line in Fig. 7(C)), which is followed by increases in surface  $\text{NO}_3$  and  $\text{TCO}_2$  concentrations (dotted line in Fig. 7(E) and (H)). The surface TALK is higher and is kept constant in the no-calcification model simulation (dotted line in Fig. 7(G)). Therefore, the  $\text{pCO}_{2\text{sea}}$  change in the no-calcification model simulation, increasing linearly with source  $\text{Si(OH)}_4$ , from 326 to 380  $\mu\text{atm}$ , is primarily controlled by the surface  $\text{TCO}_2$  change (dotted line in Fig. 7(H)

and (I)). The lower surface total phytoplankton and diatom biomass in the no-calcification model simulation results in lower export fluxes of PON or POC and  $\text{bSiO}_2$ , and a lower  $\text{bSiO}_2$ :PON export ratio than in the calcification model simulation (Figs. 7(A), (C), 9(A) and (C)).

#### 4.3. Comparison with field data

The passage of the TIWs during the JGOFS TT012 cruise gives a natural experiment of how the surface nutrients and ecosystem might respond to changes in source nutrients for comparison with the model sensitivity experiments carried out in this study (Dugdale et al., 2002). The source  $\text{Si(OH)}_4$  increased dramatically from a minimum of 6 ( $\text{mmol Si m}^{-3}$ ) in early October to a maximum of 13 ( $\text{mmol Si m}^{-3}$ ) by October 16, 1992, while the source  $\text{NO}_3$  concentration varied from a low of 10

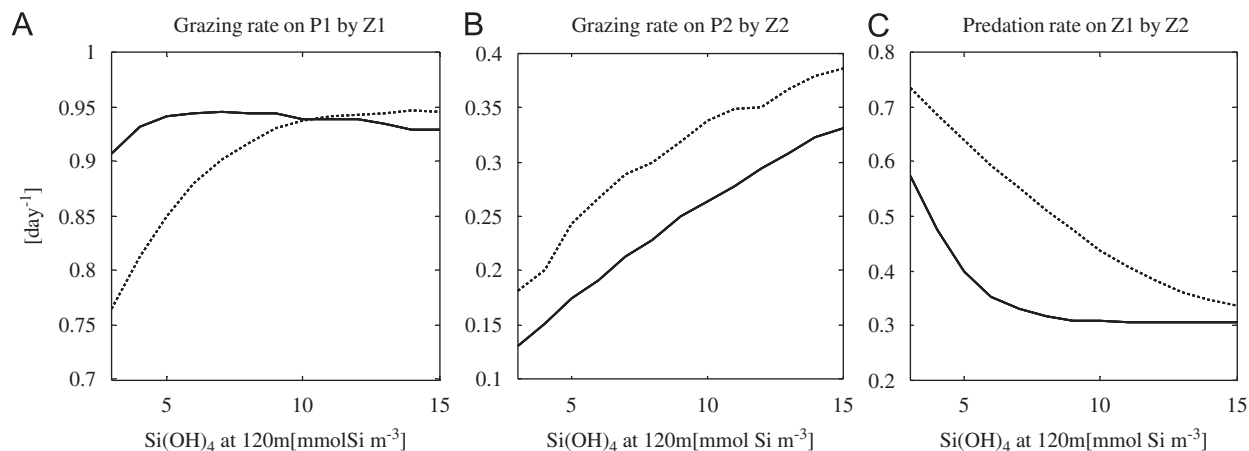


Fig. 10. Modeled specific (divided by each biomass) (A) grazing rate on picoplankton (P1) by microzooplankton (Z1) [ $\text{day}^{-1}$ ], (B) grazing rate on diatoms (P2) by mesozooplankton (Z2) [ $\text{day}^{-1}$ ], and (C) predation rate on microzooplankton (Z1) by mesozooplankton (Z2) [ $\text{day}^{-1}$ ] in the surface water vs. source  $\text{Si(OH)}_4$  concentration ( $\text{mmol Si m}^{-3}$ ) in Experiment 2. Solid lines: calcification model results. Dotted lines: no-calcification model results.

( $\text{mmol N m}^{-3}$ ) to a maximum of 14 ( $\text{mmol N m}^{-3}$ ) (Fig. 11(C) and (D)). Large increases in chlorophyll concentration and net community production, particularly for diatoms, were observed during this event (Fig. 11(A) and (B); Iriarte and Fryxell, 1995; Barber et al., 1996).

We compared the model results in Experiment 2 with the JGOFS TT012 cruise data during the passage of the TIWs (Fig. 12). Because the source  $\text{Si(OH)}_4$  concentration was enhanced by the TIWs (Fig. 12(D)), the x-axis in Fig. 12 clearly corresponds to the time series. The profiles of state variables in the surface water vs. source  $\text{Si(OH)}_4$  concentrations showed that the model results well captured the observed features during the passage of the TIWs, such as a linear surface  $\text{Si(OH)}_4$  increase with source  $\text{Si(OH)}_4$  increase (Fig. 12(B)), and maxima of surface  $\text{NO}_3$ ,  $\text{TCO}_2$ , and  $\text{pCO}_{2\text{sea}}$  at intermediate source  $\text{Si(OH)}_4$  concentrations (Fig. 12(A), (C) and (D)). The maxima of surface  $\text{NO}_3$ ,  $\text{TCO}_2$ , and  $\text{pCO}_{2\text{sea}}$  were regarded as results of increases and decreases in these state variables during and after the passage of the TIWs, respectively.

The model results with each source  $\text{Si(OH)}_4$  concentration in Experiment 2 were obtained by establishing steady states, running the model for 1000 days. Therefore, the model results in Experiment 2 may not reproduce the observed rapid increases in phytoplankton growth and chlorophyll concentration in response to the TIWs (Fig. 11(A) and (B)). We hypothesize that this is because the

dramatic changes in phytoplankton growth and biomass would be caused by non steady-state biological responses to the passage of the TIWs, which may not be reproduced by Experiment 2.

## 5. Concluding remarks

To understand factors and mechanisms controlling carbon and silicon cycling in the equatorial Pacific upwelling region, an ecosystem model with coccolithophorids and its calcification processes has been constructed. We examined biogeochemical responses to the tropical instability waves with increases of source (120 m depth)  $\text{Si(OH)}_4$  concentration. The model results revealed the top-down control (grazing by zooplankton) on phytoplankton biomass and bottom-up control (nutrient limitations, especially  $\text{Si(OH)}_4$  limitation on diatom growth) on phytoplankton growth.

The model sensitivity study to the increase of source (120 m depth)  $\text{Si(OH)}_4$  concentration shows linear increase in surface diatoms and biogenic silica export, decrease in surface picoplankton, and a maximum surface coccolithophorids at intermediate source  $\text{Si(OH)}_4$  concentrations. Surface total alkalinity and total  $\text{CO}_2$  have the minimum and maximum, respectively, at intermediate source  $\text{Si(OH)}_4$  concentrations, which produces highest  $\text{CO}_2$  release to the atmosphere with the source  $\text{Si(OH)}_4$  concentration of 7.5 ( $\text{mmol Si m}^{-3}$ ). The export ratio of PIC to particulate organic carbon (rain ratio) at 120 m depth has its maximum of 0.16

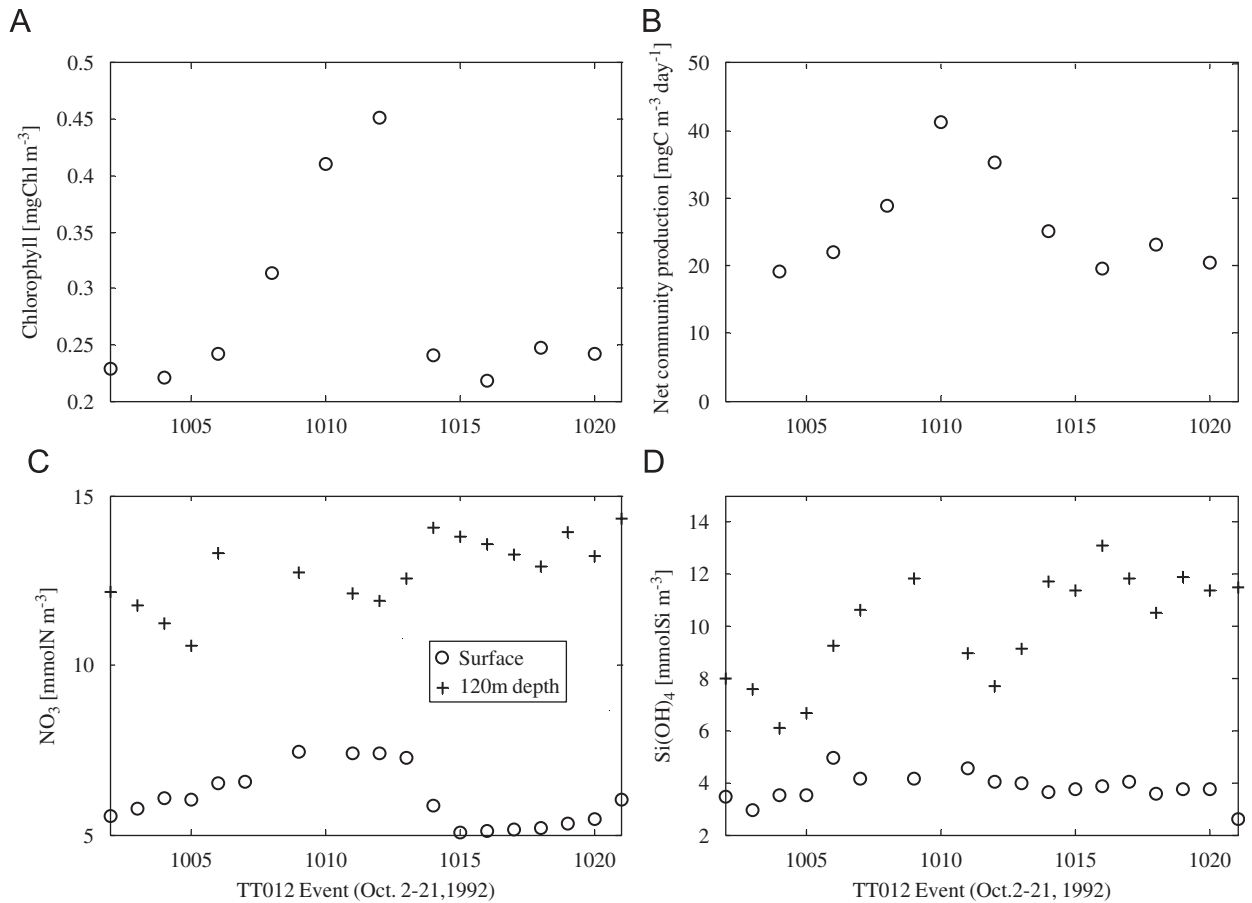


Fig. 11. (A) Chlorophyll [mgChl m<sup>-3</sup>], (B) net community production [mgC m<sup>-3</sup> day<sup>-1</sup>], (C) NO<sub>3</sub> (mmolN m<sup>-3</sup>), and (D) Si(OH)<sub>4</sub> (mmolSi m<sup>-3</sup>) at the surface (open dots) or bottom (crosses) of the euphotic zone (120 m depth) during the JGOFS EqPac Time series II (TT012) from October 2 to October 21, 1992.

with the source Si(OH)<sub>4</sub> concentration of 7.5 (mmolSi m<sup>-3</sup>), suggesting a significant PIC sedimentation in the equatorial Pacific upwelling region. Enhanced change in biogenic silica export flux than in surface diatom biomass suggests that sedimented detritus under the region acts as an amplifier of changes in surface properties.

Comparison between calcification and no-calcification model results reveals that the presence of coccolithophorids persistently elevated diatom biomass and export fluxes of detritus while it decreases total alkalinity and enhanced CO<sub>2</sub> release to the atmosphere. Large changes in the carbonate system in responses to source Si(OH)<sub>4</sub> concentrations suggest that physical forcing, such as the tropical instability waves, Kelvin waves, and La Niña, significantly affect the carbon and silicon fluxes in the region.

To understand better the carbon and silicon cycling in the equatorial Pacific upwelling region, we need more information on the processes regulating calcifiers and PIC, not only in the surface but also in the subsurface layer where the calcification is considered significant.

#### Acknowledgments

The authors thank two anonymous reviewers for improving the manuscript, and Drs. Richard Dugdale, Richard Barber, and Tsung-Hung Peng for the discussion on comparison with observations in the equatorial Pacific. Funding for this work was provided to F. Chai by a NSF Grant (OCE-0137272) and a NASA Grant (NAG5-9348) and to M. Fujii by MEXT through Special Coordination Funds for Promoting Science and Technology.

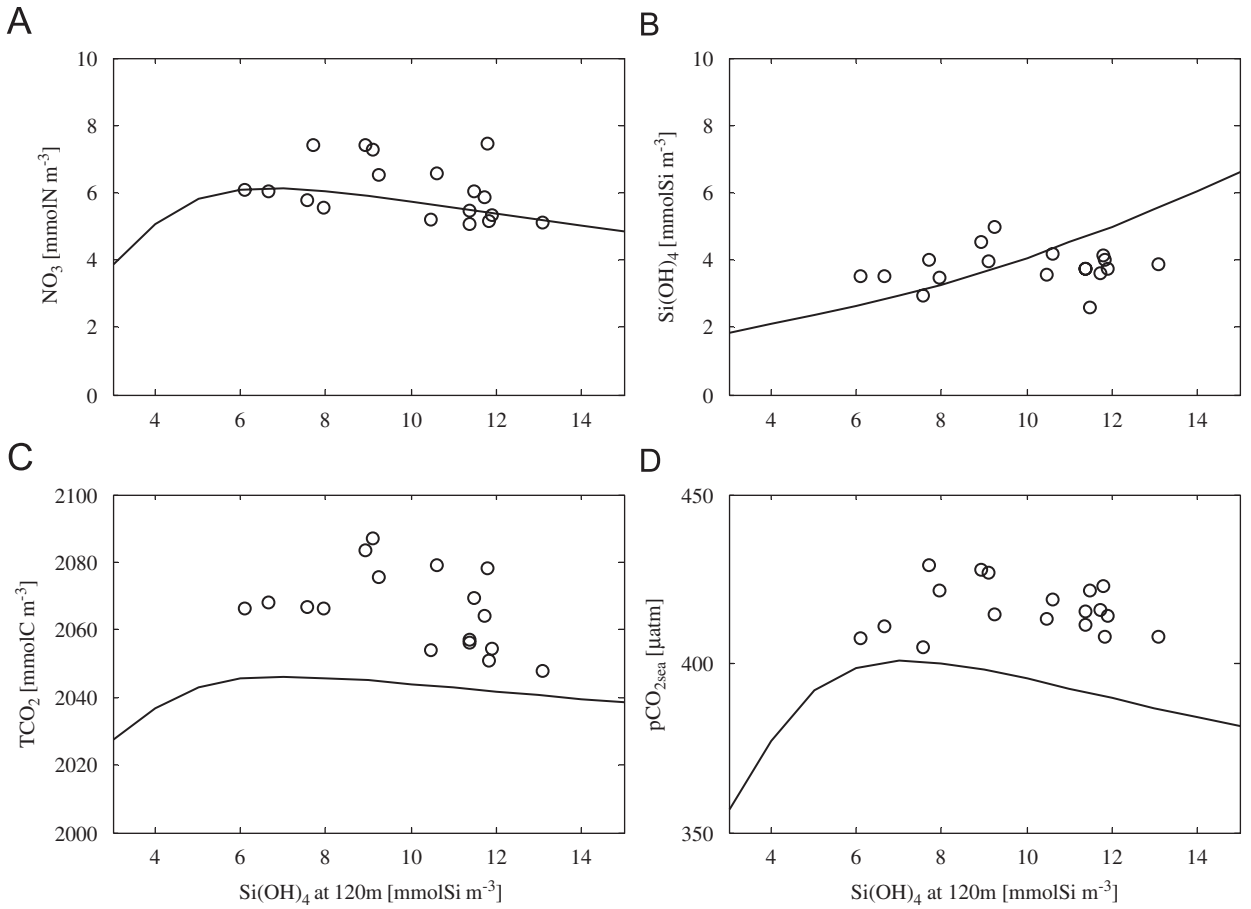


Fig. 12. Surface (A)  $\text{NO}_3$  ( $\text{mmol N m}^{-3}$ ), (B)  $\text{Si}(\text{OH})_4$  ( $\text{mmol Si m}^{-3}$ ), (C)  $\text{TCO}_2$  ( $\text{mmol C m}^{-3}$ ) and (D)  $\text{pCO}_{2\text{sea}}$  [ $\mu\text{atm}$ ] vs. source  $\text{Si}(\text{OH})_4$  concentration ( $\text{mmol Si m}^{-3}$ ). Open dots: the JGOFS EqPac Time series II (TT012) data from October 2 to October 21, 1992; Solid lines: calcification model results in Experiment 2.

## Appendix A

### A.1. Governing equations

The model equations describing each compartment all take the form

$$\frac{\partial C_i}{\partial t} [\text{mmol m}^{-3} \text{ day}^{-1}] = \text{PHYSICS}(C_i) + \text{BIOLOGY}(C_i), \quad (\text{A.1})$$

$i = 1, \dots, 13$ .

The term **PHYSICS** ( $C_i$ ) represents the contribution to the concentration change due to physical processes, including vertical advection and eddy diffusion

$$\text{PHYSICS}(C_i) [\text{mmol m}^{-3} \text{ day}^{-1}] = \underbrace{-W \frac{\partial C_i}{\partial z}}_{\text{advection}} + \underbrace{\frac{\partial}{\partial z} \left( A_{\text{Tv}} \frac{\partial C_i}{\partial z} \right)}_{\text{eddy diffusivity}}, \quad (\text{A.2})$$

where  $W$  is vertical velocity, and  $A_{\text{Tv}}$  is vertical coefficient. The term **BIOLOGY** ( $C_i$ ) represents biological sources and sinks of that compartment. In the euphotic zone (the upper 120 m), the biological terms,

BIOLOGY ( $C_i$ ) are:

$$\text{BIOLOGY}(P1)[\text{mmol N m}^{-3} \text{ day}^{-1}] = \underbrace{NP1 + RP1}_{\text{growth}} - \underbrace{G_1}_{\text{grazing by Z1}}, \quad (\text{A.3})$$

$$\text{BIOLOGY}(P2)[\text{mmol N m}^{-3} \text{ day}^{-1}] = \underbrace{NP2 + RP2}_{\text{Growth}} - \underbrace{G_2}_{\text{grazing by Z2}} - \underbrace{\gamma_3 P2}_{\text{mortality}} - \underbrace{\frac{\partial}{\partial z}(W_1 P2)}_{\text{sinking}}, \quad (\text{A.4})$$

$$\text{BIOLOGY}(P3)[\text{mmol N m}^{-3} \text{ day}^{-1}] = \underbrace{NP3 + RP3}_{\text{growth}} - \underbrace{G_5}_{\text{grazing by Z2}} - \underbrace{\gamma_6 P3}_{\text{mortality}} - \underbrace{\frac{\partial}{\partial z}(W_3 P3)}_{\text{sinking}}, \quad (\text{A.5})$$

$$\text{BIOLOGY}(Z1)[\text{mmol N m}^{-3} \text{ day}^{-1}] = \underbrace{G_1}_{\text{grazing on P1}} - \underbrace{G_3}_{\text{predation by Z2}} - \underbrace{\text{reg}_1 Z1}_{\text{excretion}}, \quad (\text{A.6})$$

$$\text{BIOLOGY}(Z2)[\text{mmol N m}^{-3} \text{ day}^{-1}] = \underbrace{\gamma_1(G_2 + G_3 + G_4 + G_5)}_{\text{fecal pellet}} - \underbrace{\text{reg}_2 Z2}_{\text{excretion}} - \underbrace{\gamma_2 Z2^2}_{\text{loss}}, \quad (\text{A.7})$$

$$\text{BIOLOGY}(\text{NO}_3)[\text{mmol N m}^{-3} \text{ day}^{-1}] = - \underbrace{NP1}_{\text{uptake by P1}} - \underbrace{NP2}_{\text{uptake by P2}} - \underbrace{NP3}_{\text{uptake by P3}} + \underbrace{\gamma_5 \text{NH}_4}_{\text{nitrification}}, \quad (\text{A.8})$$

$$\text{BIOLOGY}(\text{NH}_4)[\text{mmol N m}^{-3} \text{ day}^{-1}] = - \underbrace{RP1}_{\text{uptake by P1}} - \underbrace{RP2}_{\text{uptake by P2}} - \underbrace{RP3}_{\text{uptake by P3}} + \underbrace{\text{reg}_1 Z1 + \text{reg}_2 Z2}_{\text{excretion}} + \underbrace{\gamma_7 \text{PON}}_{\text{PON remineralization}} - \underbrace{\gamma_5 \text{NH}_4}_{\text{nitrification}}, \quad (\text{A.9})$$

$$\text{BIOLOGY}(\text{Si}(\text{OH})_4)[\text{mmol Si m}^{-3} \text{ day}^{-1}] = - \underbrace{R_{\text{SiN}}(NP2 + RP2)}_{\text{silicification}} + \underbrace{\gamma_4 b\text{SiO}_2}_{\text{bSiO}_2 \text{ dissolution}}, \quad (\text{A.10})$$

$$\text{BIOLOGY}(\text{PON})[\text{mmol N m}^{-3} \text{ day}^{-1}] = \underbrace{(1 - \gamma_1)(G_2 + G_3 + G_4 + G_5)}_{\text{fecal pellet}} - \underbrace{G_4}_{\text{grazing by Z2}} + \underbrace{\gamma_3 P2}_{\text{P2 mortality}} + \underbrace{\gamma_6 P3}_{\text{P3 mortality}} - \underbrace{\gamma_7 \text{PON}}_{\text{PON remineralization}} - \underbrace{\frac{\partial}{\partial z}(W_2 \text{PON})}_{\text{sinking}}, \quad (\text{A.11})$$

$$\text{BIOLOGY}(b\text{SiO}_2)[\text{mmol Si m}^{-3} \text{ day}^{-1}] = \underbrace{R_{\text{SiN}} G_2}_{\text{fecal pellet}} - \underbrace{\gamma_4 b\text{SiO}_2}_{\text{dissolution}} + \underbrace{\gamma_3 R_{\text{SiN}} P2}_{\text{P2 mortality}} - \underbrace{\frac{\partial}{\partial z}(W_4 b\text{SiO}_2)}_{\text{sinking}}, \quad (\text{A.12})$$

$$\text{BIOLOGY}(\text{PIC})[\text{mmol C m}^{-3} \text{ day}^{-1}] = \underbrace{R_{\text{CN}\epsilon} G_5}_{\text{fecal pellet}} - \underbrace{\gamma_8 \text{PIC}}_{\text{dissolution}} + \underbrace{\gamma_6 R_{\text{CN}\epsilon} P3}_{\text{P3 mortality}} - \underbrace{\frac{\partial}{\partial z}(W_5 \text{PIC})}_{\text{sinking}}. \quad (\text{A.13})$$

Each biological process is described in Section A.2. See Table 1 for abbreviations.

PIC production reduces TALK, and PIC dissolution increases TALK (e.g. Broecker and Peng, 1982). Brewer and Goldman (1976) demonstrated that the phytoplankton growth could affect TALK through nutrient uptake of nutrients as well. Uptake of  $\text{NO}_3$  caused an increase in TALK, whereas uptake of  $\text{NH}_4$  produced a decrease. This is because one mole of  $\text{NO}_3$  assimilation by phytoplankton generates one equivalent of strong base ( $\text{OH}^-$ ), and for  $\text{NH}_4$ , one equivalent of strong acid ( $\text{H}^+$ ). Therefore, the biological term for TALK is

written as follows:

$$\text{BIOLOGY(Talk)}[\text{mmol m}^{-3} \text{ day}^{-1}] = 2.0 \times \left\{ \underbrace{\gamma_8 \text{PIC}}_{\text{PIC dissolution}} - \underbrace{R_{\text{CN}\varepsilon}(\text{NP3} + \text{RP3})}_{\text{calcification}} \right\} - \text{BIOLOGY}(\text{NO}_3) + \text{BIOLOGY}(\text{NH}_4). \quad (\text{A.14})$$

The photosynthesis and calcification are associated with a decrease in  $\text{TCO}_2$ . The distribution of  $\text{TCO}_2$  in the water column can be given as

$$\frac{\partial(\text{TCO}_2)}{\partial t}[\text{mmol C m}^{-3} \text{ day}^{-1}] = \text{PHYSICS}(\text{TCO}_2) + \text{BIOLOGY}(\text{TCO}_2) + \text{EVASION}(\text{TCO}_2), \quad (\text{A.15})$$

$$\text{BIOLOGY}(\text{TCO}_2)[\text{mmol C m}^{-3} \text{ day}^{-1}] = \underbrace{\gamma_8 \text{PIC}}_{\text{PIC dissolution}} - \underbrace{R_{\text{CN}\varepsilon}(\text{NP3} + \text{RP3})}_{\text{calcification}} + R_{\text{CN}} \text{BIOLOGY}(\text{NO}_3) + R_{\text{CN}} \text{BIOLOGY}(\text{NH}_4), \quad (\text{A.16})$$

$$\text{EVASION}(\text{TCO}_2)[\text{mmol C m}^{-3} \text{ day}^{-1}] = E \Delta p \text{CO}_2, \quad (\text{A.17})$$

where  $E$  is the mean  $\text{CO}_2$  exchange coefficient of  $0.0391 \text{ (mmol C m}^{-3} \text{ day}^{-1} \text{ ppm}^{-1})$  at partial pressure of  $\text{CO}_2$  ( $p\text{CO}_2$ ) of 280 ppm, and  $\Delta p\text{CO}_2$  is the difference in  $p\text{CO}_2$  between surface water and atmosphere. The atmospheric  $p\text{CO}_2$  is assumed to be constant at 357 ppm (Chai et al., 2002). The EVASION ( $\text{TCO}_2$ ) term is only applied to the surface level, and is equal to zero in the water column below surface level.

## A.2. Formulation of biological processes

(Irradiance)

$$I[\text{W m}^{-2}] = I_0 \exp \left\{ -k_1 z - k_2 \int_{-z}^0 (P1 + P2 + P3) dz \right\}, \quad (\text{A.18})$$

$$I_0[\text{W m}^{-2}] = \begin{cases} I_0^{\text{Noon}} \sin\left(\frac{t-6}{12} \pi\right) & \text{(from 6 am to 6 pm),} \\ 0 & \text{(from 6 pm to 6 am),} \end{cases} \quad (\text{A.19})$$

where  $I_0^{\text{Noon}}$  is the averaged surface noontime irradiance ( $410 \text{ [W m}^{-2}\text{]};$  Chai et al., 2002).  
( $\text{NO}_3$  uptake by picoplankton)

$$\text{NP1}[\text{mmol N m}^{-3} \text{ day}^{-1}] = \mu_{1\text{max}} \underbrace{\frac{\text{NO}_3}{K_{\text{NO}_3} + \text{NO}_3}}_{\text{NO}_3 \text{ regulation}} \underbrace{e^{-\Psi_{\text{NH}_4}}}_{\text{NH}_4 \text{ inhibition}} \underbrace{(1 - e^{-(\alpha/\mu_{1\text{max}})I})}_{\text{light regulation}} P1. \quad (\text{A.20})$$

( $\text{NH}_4$  uptake by picoplankton)

$$\text{RP1}[\text{mmol N m}^{-3} \text{ day}^{-1}] = \mu_{1\text{max}} \underbrace{\frac{\text{NH}_4}{K_{\text{NH}_4} + \text{NH}_4}}_{\text{NH}_4 \text{ regulation}} \underbrace{(1 - e^{-(\alpha/\mu_{1\text{max}})I})}_{\text{light regulation}} P1. \quad (\text{A.21})$$

( $\text{NO}_3$  and  $\text{NH}_4$  uptake by diatoms)

$$\text{If } \frac{1}{R_{\text{SiN}}} \frac{\text{Si(OH)}_4}{K_{\text{Si(OH)}_4} + \text{Si(OH)}_4} > \frac{\text{NH}_4}{K_{P2\text{-NH}_4} + \text{NH}_4},$$

$$NP2[\text{mmol N m}^{-3} \text{ day}^{-1}] = \mu_{2\max} \left\{ \frac{1}{R_{\text{SiN}}} \frac{\text{Si(OH)}_4}{K_{\text{Si(OH)}_4} + \text{Si(OH)}_4} - \frac{\text{NH}_4}{K_{P2\_NH_4} + \text{NH}_4} \right\} \times \underbrace{(1 - e^{-(\alpha/\mu_{2\max})I})}_{\text{light regulation}} P2, \quad (\text{A.22})$$

$$RP2[\text{mmol N m}^{-3} \text{ day}^{-1}] = \mu_{2\max} \frac{\text{NH}_4}{K_{P2\_NH_4} + \text{NH}_4} \underbrace{(1 - e^{-(\alpha/\mu_{2\max})I})}_{\text{light regulation}} P2, \quad (\text{A.23})$$

$$\text{If } \frac{1}{R_{\text{SiN}}} \frac{\text{Si(OH)}_4}{K_{\text{Si(OH)}_4} + \text{Si(OH)}_4} \leq \frac{\text{NH}_4}{K_{P2\_NH_4} + \text{NH}_4},$$

$$NP2 = 0, \quad (\text{A.24})$$

$$RP2 = \mu_{2\max} \frac{1}{R_{\text{SiN}}} \frac{\text{Si(OH)}_4}{K_{\text{Si(OH)}_4} + \text{Si(OH)}_4} \underbrace{(1 - e^{-(\alpha/\mu_{2\max})I})}_{\text{light regulation}} P2. \quad (\text{A.25})$$

(NO<sub>3</sub> uptake by coccolithophorids)

$$NP3[\text{mmol N m}^{-3} \text{ day}^{-1}] = \mu_{3\max} \frac{\text{NO}_3}{K_{P3\_NO_3} + \text{NO}_3} \underbrace{e^{-\Psi_{\text{NH}_4}}}_{\text{NH}_4 \text{ inhibition}} \underbrace{(1 - e^{-(\alpha/\mu_{3\max})I})}_{\text{light regulation}} P3. \quad (\text{A.26})$$

(NH<sub>4</sub> uptake by coccolithophorids)

$$RP3[\text{mmol N m}^{-3} \text{ day}^{-1}] = \mu_{3\max} \frac{\text{NH}_4}{K_{P3\_NH_4} + \text{NH}_4} \underbrace{(1 - e^{-(\alpha/\mu_{3\max})I})}_{\text{light regulation}} P3. \quad (\text{A.27})$$

(Grazing on picoplankton by microzooplankton)

$$G_1[\text{mmol N m}^{-3} \text{ day}^{-1}] = G_{1\max} \frac{P1}{K_{1\text{gr}} + P1} \frac{P1}{P_{1\text{ave}}} Z1, \quad (\text{A.28})$$

food limitation
depth modification

$$P1_{\text{ave}}[\text{mmol N m}^{-3} \text{ day}^{-1}] = \frac{1}{Z'} \int_{-Z'}^0 P1 \, dz, \quad (\text{A.29})$$

where Z' is the depth of the euphotic zone (120 m).

(Grazing or predation on diatoms, coccolithophorids, microzooplankton, and PON by mesozooplankton)

$$G_2[\text{mmol N m}^{-3} \text{ day}^{-1}] = G_{2\max} \frac{\zeta_1 P2}{K_{2\text{gr}} + \zeta_1 P2 + \zeta_2 Z1 + \zeta_3 \text{PON} + \zeta_4 P3} Z2, \quad (\text{A.30})$$

$$G_3[\text{mmol N m}^{-3} \text{ day}^{-1}] = G_{2\max} \frac{\zeta_2 Z1}{K_{2\text{gr}} + \zeta_1 P2 + \zeta_2 Z1 + \zeta_3 \text{PON} + \zeta_4 P3} Z2, \quad (\text{A.31})$$

$$G_4[\text{mmol N m}^{-3} \text{ day}^{-1}] = G_{2\max} \frac{\zeta_3 \text{PON}}{K_{2\text{gr}} + \zeta_1 P2 + \zeta_2 Z1 + \zeta_3 \text{PON} + \zeta_4 P3} Z2, \quad (\text{A.32})$$

$$G_5[\text{mmol N m}^{-3} \text{ day}^{-1}] = G_{2\text{max}} \frac{\zeta_4 P_3}{K_{2\text{gr}} + \zeta_1 P_2 + \zeta_2 Z_1 + \zeta_3 \text{PON} + \zeta_4 P_3} Z_2, \quad (\text{A.33})$$

where

$$\zeta_1 = \frac{\rho_1 P_2}{\rho_1 P_2 + \rho_2 Z_1 + \rho_3 \text{PON} + \rho_4 P_3}, \quad (\text{A.34})$$

$$\zeta_2 = \frac{\rho_2 Z_1}{\rho_1 P_2 + \rho_2 Z_1 + \rho_3 \text{PON} + \rho_4 P_3}, \quad (\text{A.35})$$

$$\zeta_3 = \frac{\rho_3 \text{PON}}{\rho_1 P_2 + \rho_2 Z_1 + \rho_3 \text{PON} + \rho_4 P_3}, \quad (\text{A.36})$$

$$\zeta_4 = \frac{\rho_4 P_3}{\rho_1 P_2 + \rho_2 Z_1 + \rho_3 \text{PON} + \rho_4 P_3}. \quad (\text{A.37})$$

## References

- Archer, D., et al., 1997. A meeting place of great ocean currents: shipboard observations of a convergent front at 2°N in the Pacific. *Deep-Sea Research II* 44 (9–10), 1827–1849.
- Armstrong, R.A., Lee, C., Hedges, J.I., Honjo, S., Wakeham, S.G., 2002. A new, mechanistic model for organic carbon fluxes in the ocean based on the quantitative association of POC with ballast models. *Deep-Sea Research II* 49, 219–236.
- Bacon, M.P., Cochran, J.K., Hirschberg, D., Hammer, T.R., Fleer, A.P., 1996. Export flux of carbon at the equator during the EqPac time-series cruises estimated from <sup>234</sup>Th measurements. *Deep-Sea Research II* 43 (4–6), 1133–1153.
- Balch, W.M., Kilpatrick, K., 1996. Calcification rates in the equatorial Pacific along 140°W. *Deep-Sea Research II* 43 (4–6), 971–993.
- Barber, R.T., Sanderson, M.P., Lindley, S.T., Chai, F., Newton, J., Trees, C.C., Foley, D.G., Chavez, F.P., 1996. Primary productivity and its regulation in the equatorial Pacific during and following the 1991–1992 El Niño. *Deep-Sea Research II* 43 (4–6), 933–969.
- Bates, T.S., Cline, J.D., Gammon, R.H., Kelly-Hansen, S., 1987. Regional and seasonal variations in the flux of oceanic dimethylsulfide to the atmosphere. *Journal of Geophysical Research* 92, 2930–2938.
- Beucher, C., Tréguer, P., Hapette, A., Corvaisier, R., Metzl, N., Pochon, J., 2004. Intense summer Si-recycling in the surface Southern Ocean. *Geophysical Research Letters* 31, L09305, doi:10.1029/2003GL018998.
- Bidigare, R.R., Ondrusek, M.E., 1996. Spatial and temporal variability of phytoplankton pigment distributions in the central equatorial Pacific Ocean. *Deep-Sea Research II* 43, 809–833.
- Bidle, K.D., Azam, F., 1999. Accelerated dissolution of diatom silica by natural marine bacterial assemblages. *Nature* 397, 508–512.
- Bidle, K.D., Manganelli, M., Azam, F., 2002. Regulation of silicon and carbon preservation by temperature control on bacteria. *Science* 298, 1980–1984.
- Bidle, K.D., Brzezinski, M.A., Long, R.A., Jones, J.L., Azam, F., 2003. Diminished efficiency in the silica pump caused by bacteria-mediated silica dissolution. *Limnology and Oceanography* 48, 1855–1868.
- Brewer, P.G., Goldman, J.C., 1976. Alkalinity changes generated by phytoplankton growth. *Limnology and Oceanography* 21, 108–117.
- Broecker, W.S., Peng, T.-H., 1982. *Tracers in the Sea*. Lamont–Doherty Geological Observatory, Palisades, New York, 690pp.
- Brown, C.W., 1999. Spatial and temporal variability of *Emiliania huxleyi* blooms in SeaWiFS imagery. *Eos Transactions AGU* 80 (49 Suppl.), 153.
- Brown, C.W., Yoder, J.A., 1994. Coccolithophorid blooms in the global ocean. *Journal of Geophysical Research* 99, 7467–7482.
- Buesseler, K.O., Andrews, J.A., Hartman, M.C., Belostock, R., Chai, F., 1995. Regional estimates of the export flux of particulate organic carbon derived from thorium-234 during the JGOFS EqPac program. *Deep-Sea Research II* 42 (2–3), 777–804.
- Buitenhuis, E., Le Quéré, C., Aumont, O., Beaugrand, G., Bunker, A., Hirst, A., Ikeda, T., O'Brien, T., Piontkovski, S., Straile, D., 2006. Biogeochemical fluxes through mesozooplankton. *Global Biogeochemical Cycles* 20, GB2003, doi:10.1029/2005GB002511.
- Chai, F., Lindley, S.T., Barber, R.T., 1996. Origin and maintenance of a high nitrate condition in the equatorial Pacific. *Deep-Sea Research II* 43 (4–6), 1031–1064.

- Chai, F., Dugdale, R.C., Peng, T.-H., Wilkerson, F.P., Barber, R.T., 2002. One-dimensional ecosystem model of the equatorial Pacific upwelling system. Part I: model development and silicon and nitrogen cycle. *Deep-Sea Research II* 49, 2713–2745.
- Charlson, R.J., Lovelock, J.E., Andreae, M.O., Warren, S.G., 1987. Oceanic phytoplankton, atmospheric sulphur, cloud albedo and climate. *Nature* 326, 655–661.
- Chavez, F.R., Barber, R.T., 1987. An estimate of new production in the equatorial Pacific. *Deep-Sea Research* 34, 1229–1243.
- Chavez, F.P., Buck, K.R., Coale, K.H., Martin, J.H., DiTullio, G.R., Welshmeyer, N.A., Jacobson, A.C., Barber, R.T., 1991. Growth rates, grazing, sinking and iron limitation of equatorial Pacific phytoplankton. *Limnology and Oceanography* 36, 1816–1833.
- Coale, K.H., Johnson, K.S., Fitzwater, S.E., Gordon, R.M., Tanner, S., Chavez, F.P., Ferioli, L., Sakamoto, C., Rogers, P., Millero, F., Steinberg, P., Nightingale, P., Cooper, D., Cochlan, W.P., Landry, M.R., Constantinou, J., Rollwagen, G., Trassvina, A., Kudela, R., 1996. A massive phytoplankton bloom induced by an ecosystem-scale iron fertilization experiment in the equatorial Pacific Ocean. *Nature* 383, 495–501.
- Conkright, M.E., Antonov, J.I., Baranova, O., Boyer, T.P., Garcia, H.E., Gelfeld, R., Johnson, D.D., Locarnini, R.A., Murphy, P.P., O'Brien, T.D., Smolyar, I., Stephens, C., 2002. In: Levitus, S. (Ed.), *World Ocean Database 2001*, vol. 1: Introduction. NOAA Atlas, NESDIS 42, US Government Printing Office, Washington, DC, 167pp.
- Deuser, W.G., Ross, E.H., 1989. Seasonally abundant planktonic-foraminifera of the Sargasso Sea: succession, deep-water fluxes, isotopic compositions, and paleoceanographic implications. *Journal of Foraminiferal Research* 19, 268–293.
- Dugdale, R.C., Wilkerson, F.P., 1998. Silicate regulation of new production in the equatorial Pacific upwelling. *Nature* 391, 270–273.
- Dugdale, R.C., Wilkerson, F.P., Minas, H.J., 1995. The role of a silicate pump in driving new production. *Deep-Sea Research* 42, 697–719.
- Dugdale, R.C., Barber, R.T., Chai, F., Peng, T.-H., Wilkerson, F.P., 2002. One-dimensional ecosystem model of the equatorial Pacific upwelling system. Part II: sensitivity analysis and comparison with JGOFS EqPac data. *Deep-Sea Research II* 49, 2747–2768.
- Dunne, J.P., Murray, J.W., Aufdenkampe, A.K., Blain, S., Rodier, M., 1999. Silicon–nitrogen coupling in the equatorial Pacific upwelling zone. *Global Biogeochemical Cycles* 13 (3), 715–726.
- Fabry, V.J., 1989. Argonite production by pteropod mollusks in the subantarctic Pacific. *Deep-Sea Research* 36, 1735–1751.
- Feely, R.A., Wanninkhof, R., Goyat, C., Archer, D.E., Takahashi, T., 1997. Variability of CO<sub>2</sub> distributions and sea–air fluxes in the central and eastern equatorial Pacific during the 1991–1994 El Niño. *Deep-Sea Research II* 44 (9–10), 1851–1867.
- Flament, P.J., Kennan, S.C., Knox, R.A., Niiler, P.P., Bernstein, R.L., 1996. The three-dimensional structure of an upper ocean vortex in the tropical Pacific Ocean. *Nature* 383, 610–613.
- Foley, D.G., Dickey, T.D., McPhaden, M.J., Bidigare, R.R., Lewis, M.R., Barber, R.T., Lindley, S.T., Garside, C., Monov, D.V., McNeil, J.D., 1996. Long waves and primary productivity variations in the equatorial Pacific at 0°N, 140°W. *Deep-Sea Research II* 44 (9–10), 1801–1826.
- Francois, R., Honjo, S., Krishfield, R., Manganini, S., 2002. Factors controlling the flux of organic carbon to the bathypelagic zone of the ocean. *Global Biogeochemical Cycles* 16 (4), 1087, doi:10.1029/2001GB011722.
- Fujii, M., Chai, F., 2005. Effects of biogenic silica dissolution on silicon cycling and export production. *Geophysical Research Letters* 32, L05617, doi:10.1029/2004GL022054.
- Fujii, M., Nojiri, Y., Yamanaka, Y., Kishi, M.J., 2002. A one-dimensional ecosystem model applied to time series station KNOT. *Deep-Sea Research II* 49, 5441–5461.
- Fujii, M., Ikeda, M., Yamanaka, Y., 2005. Roles of biogeochemical processes in the carbon cycle described with a simple coupled physical–biogeochemical model. *Journal of Oceanography* 61, 803–815.
- Holligan, P.M., Viollier, M., Harbour, D.S., Camus, P., Champagne-Philippe, M., 1983. Satellite and ship studies of coccolithophorid production along a continental shelf edge. *Nature* 304, 339–342.
- Iglesias-Rodríguez, M.D., Brown, C., Doney, S. C., Kleypas, J., Kolber, D., Kolber, Z., Hayes, P.K., Falkowski, P.G., 2002. Representing key phytoplankton functional groups in ocean carbon cycle models: coccolithophores. *Global Biogeochemical Cycles* 16, doi:10.1029/001GB001454.
- Iriarte, J.L., Fryxell, G.A., 1995. Micro-phytoplankton at the equatorial Pacific (140°W) during the JGOFS EqPac time series studies: March to April 1992. *Deep-Sea Research II* 42, 559–584.
- Jiang, M.-S., Chai, F., Dugdale, R.C., Wilkerson, F.P., Peng, T.-H., Barber, R.T., 2003. A nitrate and silicate budget in the equatorial Pacific Ocean: a coupled physical–biological model study. *Deep-Sea Research II* 50, 2971–2996.
- Kessler, M.S., McPhaden, M.J., 1995. The 1991–1993 El Niño in the central Pacific. *Deep-Sea Research II* 42, 295–333.
- Ku, T.L., Luo, S., Kusakabe, M., Bishop, J.K.B., 1995. <sup>228</sup>Ra-derived nutrient budgets in the upper equatorial Pacific and the role of “new” silicate in limiting productivity. *Deep-Sea Research II* 42, 479–497.
- Landry, M.R., Barber, R.T., Bidigare, R.R., Chai, F., Coale, K.H., Dam, H.G., Lewis, M.R., Lindley, S.T., McCarthy, J.J., Roman, M.R., Stoecker, D.K., Verity, P.G., White, J.R., 1997. Iron and grazing constraints on primary production in the central equatorial Pacific: an EqPac synthesis. *Limnology and Oceanography* 42, 405–418.
- Landry, M.R., Ondrusek, M.E., Tanner, S.J., Brown, S.L., Constantinou, J., Bidigare, R.R., Coale, K.H., Fitzwater, S., 2000. Biological response to iron fertilization in the eastern equatorial Pacific (IronExII). I. Microplankton community abundances and biomass. *Marine Ecology Progress Series* 201, 27–42.
- Le Borgne, R., Brusset, C., Eldin, G., Radenac, M.-H., Rodier, M., 1995. Campagne océanographique FLUPAC à bord du N.O. l'ATALANTE. Du 23 septembre au 29 octobre 1994. Recueil des données, Tome 1. ORSTOM, Nouméa, Archives Sciences de la Mer, Océanographique, No. 1.
- Le Borgne, R., Langlade, M.J., Polidori, P., Rodier, M., 1998. Campagne océanographique EBENE à bord du N.O. l'ATALANTE. Du 21 octobre au 20 novembre 1996. Recueil des données, Tome 1. ORSTOM, Nouméa, Archives Sciences de la Mer, Océanographique, No. 3.

- Levitus, S., Reid, J.L., Conkright, M.E., Najjar, R., 1993. Distribution of nitrate, phosphate and silicate in the world ocean. *Progress in Oceanography* 31, 245–273.
- Leynaert, A., Treguer, P., Lancelot, C., Rodier, M., 2001. Silicon limitation of biogenic silica production in the Equatorial Pacific. *Deep-Sea Research I* 48, 639–660.
- Loukos, H., Frost, B., Harrison, D.E., Murray, J.W., 1997. An ecosystem model with iron limitation of primary production in the equatorial Pacific at 140°W. *Deep-Sea Research II* 44 (9–10), 2221–2249.
- Luo, S., Ku, T.-L., Kusakabe, M., Bishop, J.K.B., Yang, Y.-L., 1995. Tracing particle cycling in the upper ocean with <sup>230</sup>Th and <sup>228</sup>Th: An investigation in the equatorial Pacific along 140°W. *Deep-Sea Research II* 42 (2–3), 805–829.
- Martin, J.H., et al., 1994. Testing the iron hypothesis in ecosystems of the equatorial Pacific Ocean. *Nature* 371, 123–129.
- McCarthy, J.J., Garside, C., Nevins, J.L., Barber, R.T., 1996. New production along 140W in the equatorial Pacific during and following the 1992 El Niño event. *Deep Sea Research II* 43 (4–6), 1065–1093.
- Milliman, J.D., Troy, P.J., Balch, W.M., Adams, A.K., Li, Y.-H., MacKenzie, F.T., 1999. Biologically mediated dissolution of calcium carbonate above the chemical lysocline? *Deep-Sea Research I* 46, 1653–1669.
- Moore, J.K., Doney, S.C., Kleypas, J.A., Glover, D.M., Fung, I.Y., 2002. An intermediate complexity marine ecosystem model for the global domain. *Deep-Sea Research II* 49, 403–462.
- Murray, J.W., Johnson, E., Garside, C., 1995. A US JGOFS process study in the equatorial Pacific (EqPac): Introduction. *Deep-Sea Research II* 42 (2–3), 275–293.
- Murray, J.W., Young, J., Newton, J., Dunne, J., Chapin, T., Paul, B., McCarthy, J.J., 1996. Export flux of particulate organic carbon from the central equatorial Pacific determined using a combined drifting trap-<sup>234</sup>Th approach. *Deep-Sea Research II* 43 (4–6), 1095–1133.
- Murray, J.W., Leborgne, R., Dandonneau, Y., 1997. JGOFS studies in the equatorial Pacific. *Deep-Sea Research II* 44 (9–10), 1759–1763.
- Najjar, R.G., Orr, J.C., 1998. Design of OCMIP-2 simulations of chlorofluorocarbons, the solubility pump and common biogeochemistry. 19pp.
- Orr, J., et al., 2005. Anthropogenic ocean acidification over the twenty-first century and its impact on calcifying organisms. *Nature* 437, doi:10.1038/nature04095.
- Pasquer, B., Laruelle, G., Becquevort, S., Schoemann, V., Goosse, H., Lancelot, C., 2005. Linking ocean biogeochemical cycles and ecosystem structure and function: results of the complex SWAMCO-4 model. *Journal of Sea Research* 53 (1–2), 93–108.
- Pätsch, J., Kühn, W., Radach, G., Santana Casiano, J.M., Gonzalez Davila, M., Neuer, S., Freudenthal, T., Llinas, O., 2002. Interannual variability of carbon fluxes at the North Atlantic Station ESTOC. *Deep-Sea Research II* 49, 253–288.
- Price, N.M., Ahner, B.A., Morel, F.M.M., 1994. The equatorial Pacific Ocean: grazer controlled phytoplankton populations in an iron-limited ecosystem. *Limnology and Oceanography* 39, 520–534.
- Rainbault, P., Slawyk, G., Boudjellal, B., Coatanoan, C., Conan, P., Coste, B., Garcia, N., Moutin, T., Pujo-Pay, M., 1999. Carbon and nitrogen uptake and export in the equatorial Pacific at 150°W: evidence of an efficient regenerated production cycle. *Journal of Geophysical Research* 104, 3341–3356.
- Riebesell, U., Zondervan, I., Rost, B., Tortell, P.D., Zeebe, R.E., Morel, F.M.M., 2000. Reduced calcification of marine plankton in response to increased atmospheric CO<sub>2</sub>. *Nature* 407, 364–367.
- Rodier, M., Le Borgne, R., 1997. Export flux of particles at the equator in the western and central Pacific Ocean. *Deep-Sea Research II* 44, 2085–2113.
- Sanderson, M.P., Hunter, C.N., Fitzwater, S.E., Gordon, R.M., Barber, R.T., 1995. Primary productivity and trace metal contamination measurements from a clean rosette system versus ultra-clean Go-Flo bottles. *Deep-Sea Research II* 42, 431–441.
- Sarmiento, J.L., Dunne, J., Gnanadesikan, A., Key, R.M., Matsumoto, K., Slater, R., 2002. A new estimate of the CaCO<sub>3</sub> to organic carbon export ratio. *Global Biogeochemical Cycles* 16, doi:10.1029/2002GB001919.
- van Andel, T.H., 1975. Cenozoic history and paleoceanography of the central equatorial Pacific Ocean. *Memoirs of the Geological Society of America* 143, 1–134.
- Walsh, J.J., 1976. Herbivory as a factor in patterns of nutrient utilization in the sea. *Limnology and Oceanography* 21, 1–13.
- Westbroek, P., Youn, P.R., Linschooten, K., 1989. Coccolith production (biomineralization) in the marine alga *Emiliania huxleyi*. *Journal of Protozoology* 36, 368–373.
- Wyrtki, K., 1981. An estimate of equatorial upwelling in the Pacific. *Journal of Physical Oceanography* 11, 1205–1214.
- Yamanaka, Y., Tajika, E., 1996. The role of the vertical fluxes of particulate organic matter and calcite in the carbon cycle: studies using an ocean biogeochemical general circulation model. *Global Biogeochemical Cycles* 10, 361–382.
- Yamanaka, Y., Yoshie, N., Fujii, M., Aita, M.N., Kishi, M.J., 2004. An ecosystem model coupled with nitrogen-silicon-carbon cycles applied to station A7 in the northwestern Pacific. *Journal of Oceanography* 60, 227–241.